THESIS

EVALUATING THERMAL EFFICIENCY AND ECONOMIC IMPACTS IN SUPPLYING ENERGY DEMANDS FOR DIRECT AIR CAPTURE

Submitted by

Madeleine Hope Siegel

Department of Mechanical Engineering

In partial fulfillment of the requirements

For the Degree of Master of Science

Colorado State University

Fort Collins, Colorado

Fall 2024

Master's Committee:

Advisor: Todd Bandhauer

Jason Quinn
Daniel Herber

ABSTRACT

EVALUATING THERMAL EFFICIENCY AND ECONOMIC IMPACTS IN SUPPLYING ENERGY DEMANDS FOR DIRECT AIR CAPTURE

Direct Air Capture (DAC) technologies that remove CO_2 directly from the atmosphere are needed to meet international goals of limiting atmospheric temperature increase before 2100. Operating costs, including the cost of energy inputs, currently limit the rapid deployment of DAC systems. An abundance of untapped and abandoned geothermal resources provides an opportunity to utilize this thermal energy beneath the Earth's surface to reduce the financial and energy costs of DAC. In this study, thermodynamic models of applicable renewable energy scenarios for fulfilling heating and electrical requirements of DAC were analyzed using ASPEN Plus. Individual components were optimized within the geothermal-DAC coupled systems to quantify specific costs of implementation. The results were integrated into a techno-economic analysis (TEA) to provide a holistic perspective to optimize DAC coupled renewable energy systems. The levelized cost of energy (LCOE) for DAC was reduced from \$175/t-CO_2 removed to as low as \$66/t-CO_2 removed, guiding large-scale deployment of DAC, and supporting decision-making in the future.

ACKNOWLEDGEMENTS

I would first like to thank Dr. Todd Bandhauer for giving me the opportunity to come to Fort Collins for an REU that introduced me to research at the Powerhouse. I was elated when he invited me to join the REACH CoLab for my graduate experience. The knowledge and experience I've gained from this lab have taught me exponentially. Dr. Bandhauer encouraged me to explore my passions outside of just my curriculum by doing a graduate certificate in the business school along with a Research-to-Market program. My experience gained from this lab makes me confident in my future career.

I would also like to thank Joe Huyett, who has mentored me closely over the past 2.5 years and I truly would not be in this position without his knowledge, expertise, and mentorship. Joe has supported me in so many ways and has expanded my experience in this lab that I will always be grateful for. I also extend my thanks to the other graduate students and researchers in the lab. Having a supportive community around me has made graduate school such a positive experience and it's allowed me to develop not only as an engineer but as an individual. The ski trips, post work happy hours, taco Fridays, and morning mountain bike rides helped keep me sane and I'm grateful to have made lifelong friends. Bella Amyx, Taylor Stoll, Katie Plese, and Brandi Grauberger will always be my "Lab Ladies" and have given me a strong support group as fellow women in STEM. Victor Reyes-Flores, Fred Schmid, and Ben Platt I could always count on for a laugh or a quick break watching the planes on flightradar24 when grad school was feeling overwhelming.

I also want to thank all my friends back home who bought flights to visit me and gave me a place to stay when I missed them. Also, to all my new friends in Fort Collins who made this

adjustment across the country feel effortless by welcoming me with open arms. To Jeff – you taught me the fragility of life and the importance of expressing gratitude for those around me. You always believed in me, and I know you'd be proud of where I am today.

Finally, I would like to extend a heartfelt thanks to my mom, dad, Sage, Mason, Aunt Linda, Uncle Nick, and my wonderful partner Field. Through all the ups and downs the past two years had to offer, I always knew you guys had my back. I've felt the unconditional love and support every step of the way, and I couldn't have done it without you all.

TABLE OF CONTENTS

LIST OF TABLES

LIST OF FIGURES

NOMENCLATURE

Variables	Description	Units/Formula
Q	Heat duty	kW
T	Temperature	°C
$\dot{m}$	Mass flow rate	kg/s
$\dot{W}$	Power	kW
η	Efficiency	-
Cp	Specific heat	kJ kg^{-1} $°C^{-1}$
EF	Emissions factor	gCO_2/kWh

Subscripts and Superscripts

Reinj	Reinjection to reservoir
Res	Geothermal reservoir temperature
CW	Cooling water
Turb	Turbine
B	Brine
H	Hot side
C	Cold side
th	Thermal
e	Electrical
Cond	Condenser
ORC	Organic Rankine cycle
n	Total lifetime
t	Year of lifetime
i	Discount Rate
A_t	Annual total cost, per year t
$M_{t,CO2}$	Total CO_2 removed in tonnes/year
Grid	Electricity grid

CHAPTER 1. Introduction

1.1. Motivation for Carbon Capture and Storage

To meet the Intergovernmental Panel on Climate Change (IPCC) goal of limiting an atmospheric temperature increase of 1.5°C by 2050, an estimated 328 billion tonnes of CO_2 need to be removed from the atmosphere between 2020 and 2100, with 29 billion tonnes via direct air carbon capture and storage (DACCS) [1]. Significant emerging technologies include the use of DAC which will be pivotal in achieving climate goals. The Paris Agreement, adopted by 195 nations in December 2015, aims to strengthen the global response and efforts towards the threat of climate change [2]. The agreement outlines an effort to hold the increase of the global average temperature for pre-industrial levels at less than 2°C [3]. Figure 1-1 shows the important role of CO_2 removal in climate change mitigation strategies to achieve the goals highlighted in the agreement.

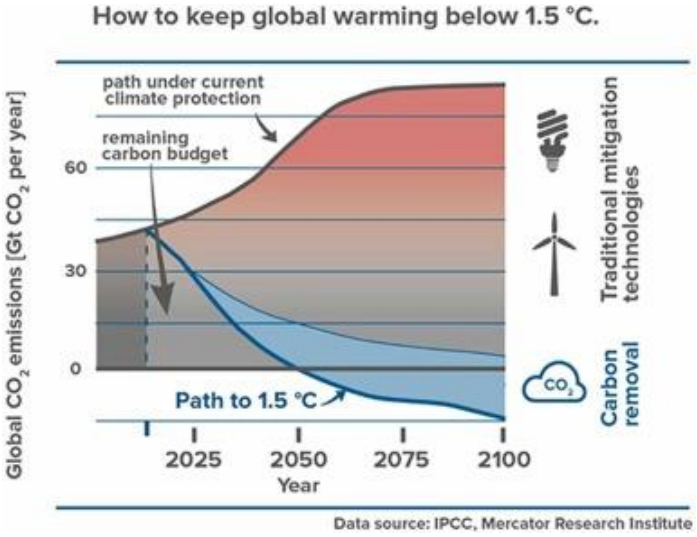

Figure 1-1: Carbon dioxide removal (CDR) impact on climate change mitigation [4].

Currently in ambient air, carbon dioxide (CO_2) is distributed across the globe at concentrations around 425.55 parts per million [4]. Being able to remove this distributed CO_2 from the atmosphere requires a fast transition of energy systems that are cost-competitive, and renewable, including large-scale deployment of CDR technology. According to a report by the International Energy Agency (IEA), CO_2 needs to be removed from the atmosphere at a rate of 10 Gigatonnes (billions of tonnes) of CO_2 per year by 2050 [5] to achieve the goals outlined in the Paris Agreement. Hanna et al. showed through scenario modeling that DAC can not only limit the growth of the warming curve but can also provide warming reversal if society overshoots the goal [1]. Adoption of CDR approaches is crucial to meet these objectives, including land-based (e.g., soil carbon sequestration), ocean-based (e.g., ocean alkalinity enhancement), geochemical-based (enhanced rock weathering), and chemical-based solutions, (e.g., DAC) [6]. There are companies active in the DAC industry, utilizing different technologies in various markets. Carbon Engineering (CE), based in Canada, uses liquid alkali metal oxide sorbents with regeneration at around 800°C. CE uses natural gas to power their DAC processes, capturing the flue gas of the combusted natural gas in addition to atmospheric air capture [4]. Climeworks uses an adsorption/desorption process. CO_2 adsorption is performed under ambient conditions and CO_2 desorption is performed through a temperature vacuum-swing process under regeneration temperatures of 80°C-120°C. Climeworks commissioned the world's first commercial DAC plant in Hinwil, Switzerland in 2017 and has commissioned one in Iceland as well [7]. Climeworks currently has 17 DAC plants with three more in planning and production, as the company employs the largest team of DAC experts to date. These companies lead the way to widespread DAC implementation for decades to come, taking the forefront of meeting IPCC goals by reducing atmospheric CO_2 emissions.

1.2. Geothermal Integration with DAC

DAC is a process that captures CO_2 directly from the air to then be stored underground or utilized in commercial products. The two main DAC technology pathways include solid sorbent and liquid solvent processes. Solid sorbent is most applicable for this study as the process adsorbs CO_2 on the surface of solid materials and then releases it under low temperature heat [8]. Geothermal energy is suitable to provide this heat as many reservoirs are available in the low temperature range needed for desorption. DAC requires approximately 80% of its energy in the form of heat and the remaining 20% as electricity [9], [10]. Geothermal heat energy can produce carbon-free electricity through use of an organic Rankine cycle (ORC), which evaporates a working fluid to drive a turbine generator. However, producing electricity using geothermal heat is only about 12% efficient, with a lower conversion efficiency than all alternative thermal plants [11]. Using heat as heat instead of converting it to electricity can be a more effective approach in low temperature systems where the conversion efficiency is limited. In a geothermal-DAC coupled system, using the highest exergy portion of the brine heat for the ORC and the lower exergy portion directly as heat for DAC could be a more efficient use of the total enthalpy in the brine.

Geothermal energy is widely available throughout the United States, with high electric power generation potential from both identified and undiscovered conventional geothermal resources in addition to many enhanced geothermal systems (EGS) [12]. According to the report by the United States Geological Survey and shown in Figure 1-2, there is a mean potential of 9,057 MW_e in the western United States for identified resources, 30,033 MW_e for undiscovered resource potential, and 517,800 MW_e for EGS[13]. The highest geothermal electric power potentials are in California with 5,404 MW_e, 11,340 MW_e and 48,100 respectively, and Nevada with 1,391 MW_e, 4,364 MW_e, and 102,800 MW_e respectively. Based on the low conversion efficiency, the amount of thermal energy these estimates represent is substantially higher still.

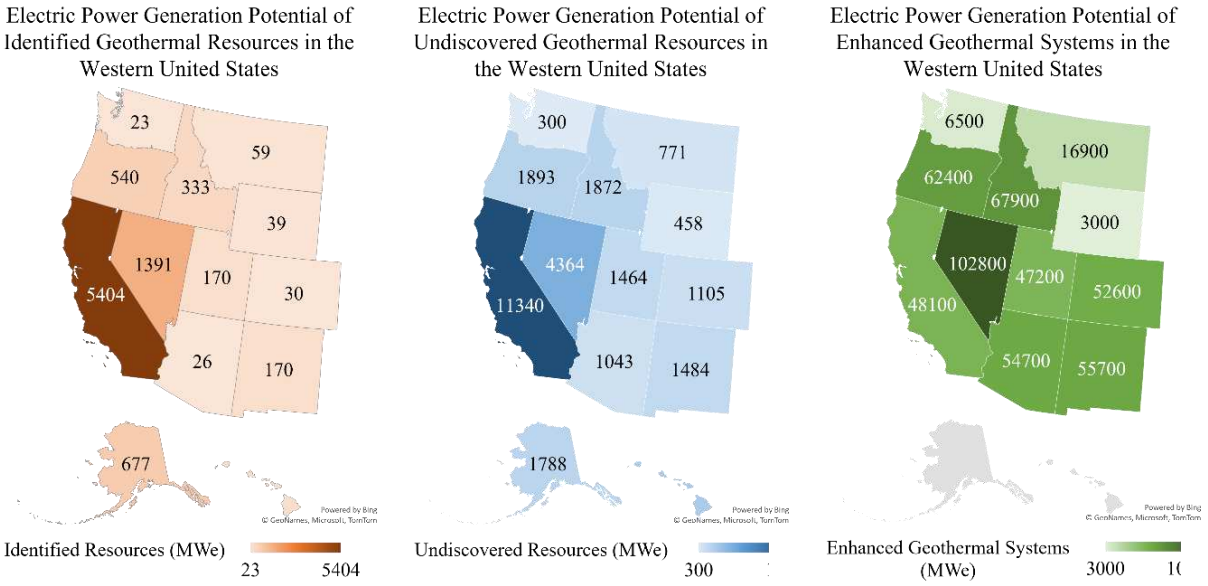

Figure 1-2: Electric power generation potential of (A) Identified Geothermal Resources, (B) Undiscovered Geothermal Resources, and (C) Enhanced Geothermal Systems in the Western United States.

Specifically in Nevada, there are reservoirs that enable high scalability of geothermal potential throughout the state. Figure 1-3 shows a map developed by Zehner et. al showing geothermal potential by location and reservoir temperature across the state, emphasizing a geographical region where DAC can be technologically feasible.

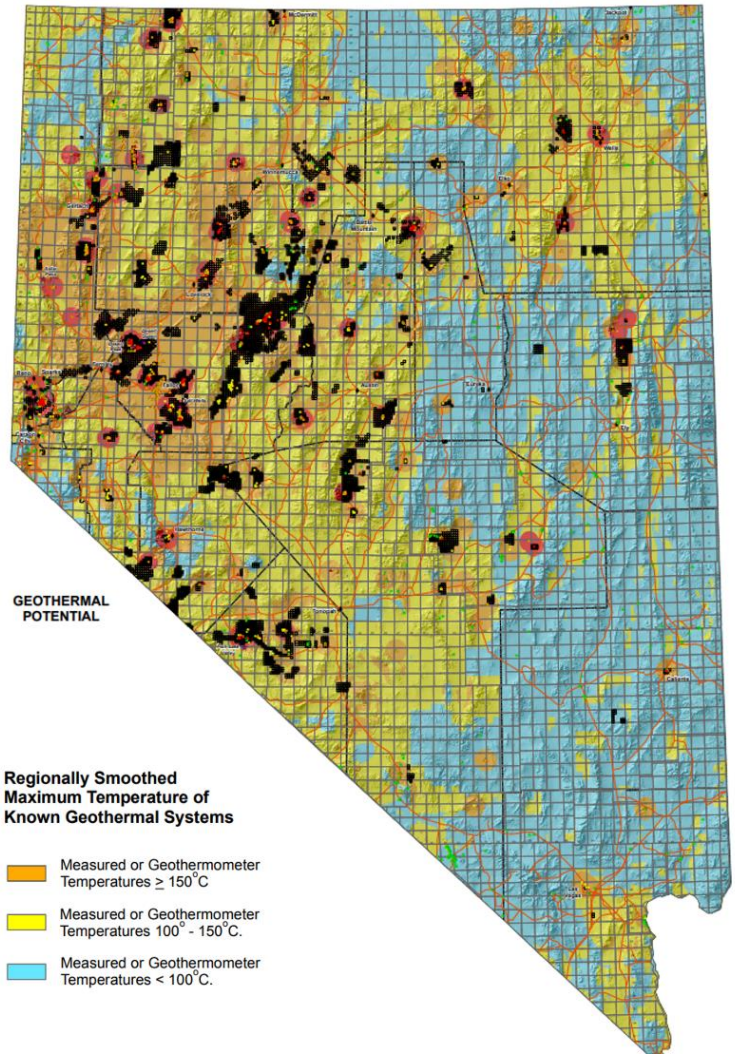

Figure 1-3: Geothermal temperatures of known geothermal systems in Nevada [14].

Geothermal reservoirs in Nevada present promising opportunities for DAC. Areas indicated with temperatures exceeding 150°C (highlighted in orange) and those between 100°C – 150°C (highlighted in yellow) are potential candidates for geothermal-DAC integration. These temperature ranges align with thermal requirements for solid sorbent DAC technologies, demonstrating a strong potential to leverage this geothermal heat to meet energy demands of the DAC process efficiently.

Renewable energy for use in DAC offers a sustainable use of resources when removing carbon dioxide from the air. To understand the economic effectiveness of utilizing these resources, a down selection of scenarios was selected based on an initial economic assessment to compare a comprehensive view of DAC implementation in the United States. Grid dependent options and fully independent solutions were evaluated to present options for varying resources and needs. Scenarios are shown in Table 1-1.

Table 1-1: Representative scenarios for DAC using renewable energy sources.

Configuration	DAC ?	Heat Source	Electricity Source	CAPEX	OPEX	Fully Independent?	Cost Reference
1. Geothermal Energy to Grid	X	Geothermal Heat	Organic Rankine Cycle	High	Medium	✓	[15]
2. Geothermal+Grid Electricity	✓	Geothermal Heat	Electricity Grid	Medium	High	X	[15], [16]
3. Geothermal+ORC	✓	Geothermal Heat	Organic Rankine Cycle	High	Medium	✓	[15]
4. Geothermal+VPPA	✓	Geothermal Heat	Virtual Power Purchase Agreement	Medium	High	X	[15]
5. VPPA	✓	Virtual Power Purchase Agreement	Virtual Power Purchase Agreement	Low	High	X	[17], [18]
6. Geothermal+Firm Renewables	✓	Geothermal Heat	Solar PV + Battery Storage	High	Medium	✓	[15]
7. Solar+Battery	✓	Solar PV + Battery Storage	Solar PV + Battery Storage	High	Medium	✓	[15]

Using VPPA's for DAC proves to be an economical option with a LCOE for DAC at \$80/t-CO_2 removed (Appendix A), directly compared against \$120/t-CO_2 removed for Geothermal+ORC,

$115/t-$CO_2$ removed for Geothermal+Firm Renewables, and $175/t-$CO_2$ removed for Solar+Battery. Minimal CAPEX investments and only OPEX costs with set contract prices makes this case attractive when paired with DAC technologies. However, analyzing grid-dependent options for DAC was deemed impractical due to concerns about additionality and dependency on high-emission, variable-cost electricity sources for reliability. Substituting clean electricity that could be used to assist in decarbonizing the grid should include having to account for the lost CO_2 reduction of the grid. This would decrease the overall CO_2 removed resulting in higher levelized cost values in these specific scenarios. Additionally, a new report from LevelTen PPA Price Index reports solar PPA prices climbed 8.5% in the first quarter of 2023 [19], signifying that VPPA for future DAC implementation will continuously increase costs and should not be solely relied upon. Therefore, only fully independent solutions were evaluated in this analysis.

1.3. Research Objectives

This study examines the thermodynamic opportunities and limitations of pairing DAC with geothermal heat, while assessing the impact of reservoir temperature and regeneration temperature on total CO_2 removal. Figure 1-4 outlines the 4 renewable energy scenarios evaluated throughout the study, showing where the electricity and thermal requirements are being sourced from.

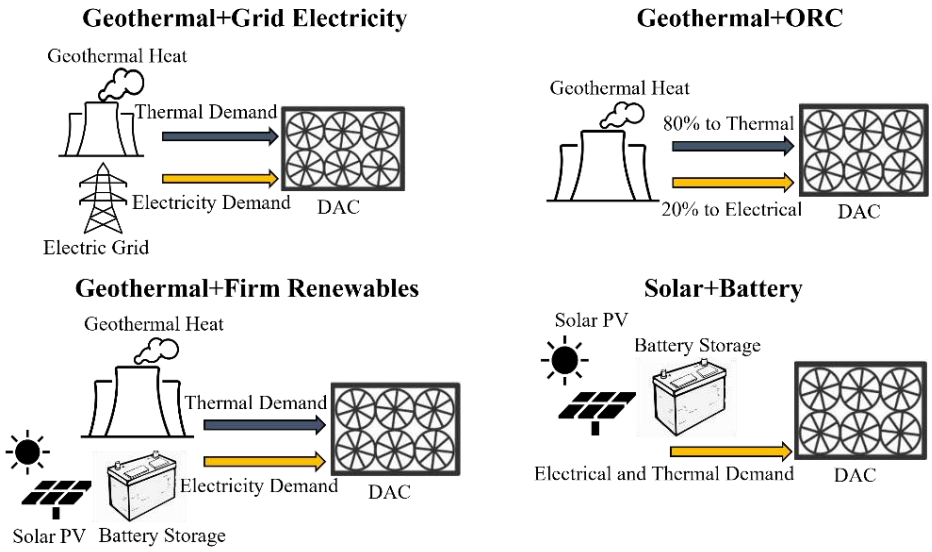

Figure 1-4: Renewable energy scenarios evaluated in study for supplying energy demands for DAC.

Geothermal reservoir temperatures tested are 125°C, 145°C, 165°C, 185°C, and 205°C. DAC regeneration temperatures tested are 80°C, 100°C, and 120°C. Geothermal results were compared against other renewable energy sources to find optimal opportunities across these different parameters.

The Geothermal+Grid Electricity case was included as a direct comparison to understand drawbacks with DAC implementation when needing to account for electric grid emissions, along with sourcing electricity that has markups dependent on demand times. Evaluating these scenarios gives a techno-economic framework for geothermal-DAC.

Current studies have shown using geothermal energy for DAC to be an economical option compared to other energy sources. Figure 1-5 presents a simplified model of the geothermal-DAC coupled system intending to remove CO_2 from the atmosphere. The study focuses on the boxed region, minimizing the LCOE for the DAC process comparing various energy sources to meet demands of the system.

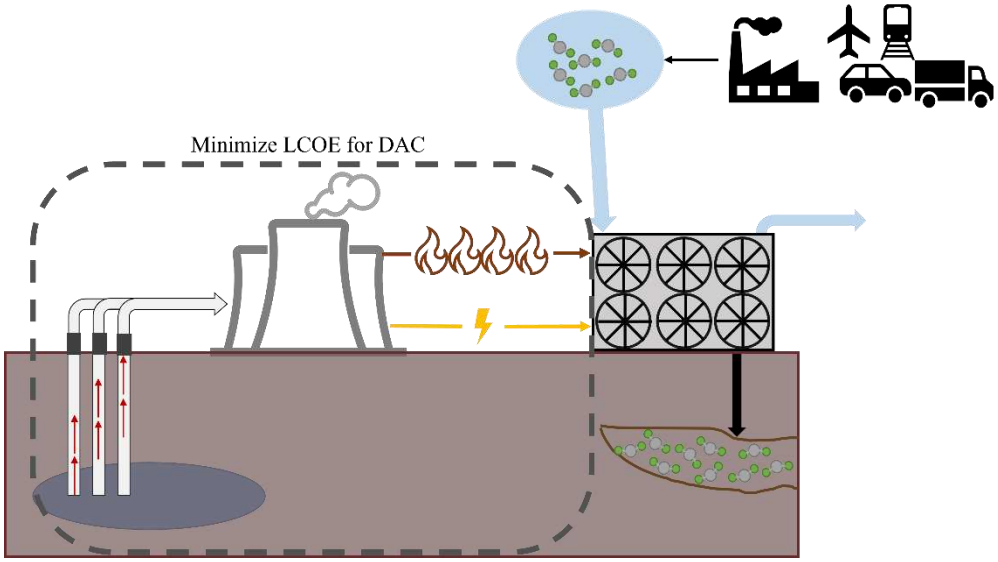

Figure 1-5: Simplified geothermal-DAC coupled system for atmospheric CO_2 removal.

This study further examines the thermodynamic opportunities and limitations of pairing DAC with geothermal heat, while assessing the impact of reservoir temperature and regeneration temperature on total CO_2 removal. Developing thermodynamic models for various renewable energy cases, including geothermal-DAC coupled systems and optimizing the individual components in an ASPEN Plus model provides a detailed analysis of its feasibility. The results were then integrated into a technoeconomic analysis, providing an evaluation of various energy input cases for DAC. Results were compared against other applicable renewable energy sources to find economic opportunities across different parameters to identify long term deployment opportunities for CDR.

1.4. Thesis Organization

This thesis expands on concepts of implementing geothermal energy for DAC processes compared to other energy sources. Chapter 2 provides an analysis of the existing literature, with a review on current studies and identifying relevant gaps in the work. Chapter 3 outlines the process behind implementing the geothermal-DAC coupled system for thermodynamic modeling

and how the data was implemented into the economic model, followed by a comparison of levelized cost values across various renewable energy sources to fulfil DAC energy requirements. Chapter 4 discusses the modeling results and the highlights of the research. Finally, Chapter 5 summarizes the main takeaways of the study and outlines some limitations along with recommendations for future work.

Appendix A contains the discounted cash flow for the VPPA case, which was one of the cases explored in initial evaluations but not continued throughout the study due to additionality issues highlighted earlier in this chapter. Appendix B provides the discounted cash flows for the cases explored throughout the modeling results. The Solar+Battery case is provided in the main text of the study due to it being the "baseline case" for renewable energy for DAC without the use of geothermal energy.

CHAPTER 2. Literature Review

The present study will focus on utilizing geothermal energy for DAC thermal and electrical requirements compared to other renewable energy sources. DAC requires a significant amount of energy to strip CO_2 from the atmosphere. This energy is in the form of 80% heating and 20% electrical. Finding renewable energy sources that can fulfil this requirement in an efficient and cost-effective way is vital to the success of DAC implementation. The study focuses on identifying applicable energy sources for DAC and quantifies the economic feasibility while utilizing component-based thermodynamic modeling for multiple configurations and cases.

A review is provided on the relevant literature for thermodynamic and economic studies of DAC along with geothermal-DAC coupled systems. After the review of the literature, the primary gaps in the research will be identified to provide context and reasoning for the present work. The specific aims will be presented, informed by the literature gaps that will highlight the need for the present research done in this study.

2.1. Carbon Dioxide Removal Technologies

CDR technologies are necessary to achieve climate goals outlined in the Paris Agreement. Many types of carbon capture exist in the world around us today, and many are needing improvements before large scale deployment can be feasible. CDR has a wide range of approaches including DAC, soil carbon sequestration, biomass carbon removal and storage, enhanced mineralization, ocean-based CDR, and afforestation/reforestation [20]. Figure 2-1 highlights the many CDR pathways used presently, coupled with CO_2 storage opportunities to create a full cycle illustration of removal with storage-based solutions.

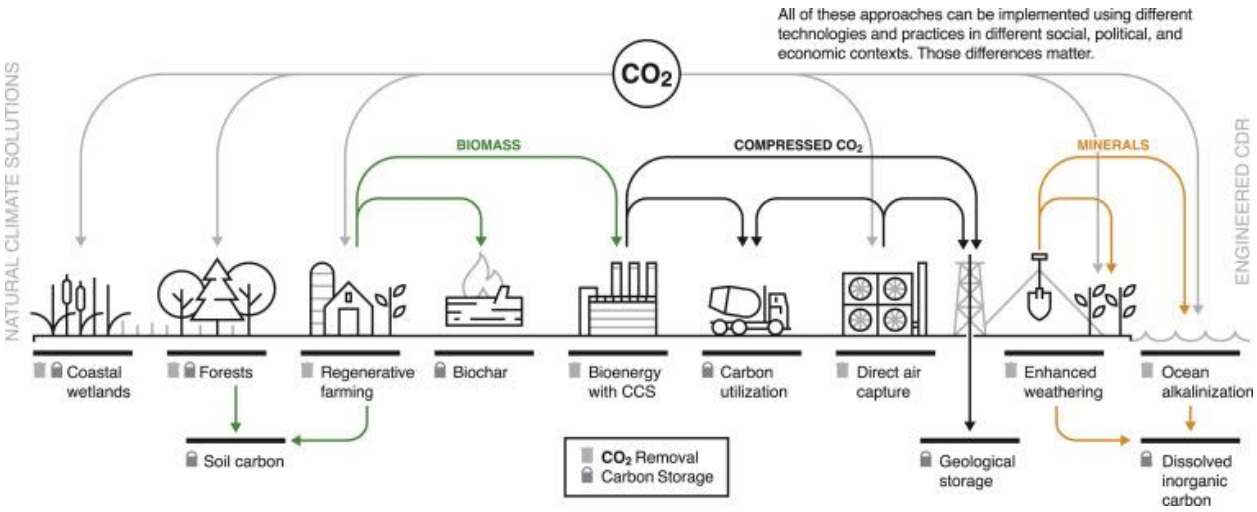

Figure 2-1: CDR pathways to CO_2 removal and carbon storage opportunities [21].

Engineered CO_2 removal technologies are essential when it comes to CDR as it directly addresses excess CO_2 already dispersed in the atmosphere. Nature-based carbon storage is naturally occurring and readily available, however it can have adverse effects as the carbon stored in forests or soil can be released back into the atmosphere under certain conditions. Forests act as both carbon sinks and potential sources of rapid emissions due to unforeseen natural disturbances, including fires, insect infestations, and human activities. Ultimately nature-based carbon storage is important, but it can't reverse the accumulated effects. Post combustion carbon capture and storage is necessary because it prevents newly emitted CO_2 from entering the atmosphere, however it doesn't deal with the existing CO_2 accumulated from years of emissions. Relying on CO_2 removal technologies (highlighted as the trashcan in Figure 2-1) like DAC, alongside nature-based storage solutions is crucial to achieve climate goals. These engineered CO_2 removal technologies permanently store emissions that are already dispersed throughout the atmosphere. When these technologies are paired with deployment of mitigation strategies, CDR will allow emissions to be addressed from many heavily emitting sectors including residential and commercial (31%), industrial (30%), transportation (29%), and agriculture (10%) [22].

DAC will be the focused technology of the study presented. There are two main types of DAC currently being scaled commercially: solid sorbent and liquid solvent. Liquid solvent DAC includes aqueous-based solutions including alkaline solutions that are widely used in these types of systems. Liquid solvent DAC solutes are only present up to 30 wt. percent in the solution due to the nature of the substance, limiting the number of interactions it can have with the CO_2 molecules [23]. Additionally, they require high temperatures for regeneration. Carbon Engineering has developed an aqueous DAC system that requires around 900°C regeneration temperatures [24]. Alternatively, solid sorbent DAC allows the base to chemically bind to the porous material of the sorbent used, increasing the surface area and therefore DAC capacity. These DAC units require electricity and heat at around 80°C – 120°C for CO_2 capture and regeneration [4], [9], [25]. Fasihi et al. outlined current companies pursuing solid sorbent DAC with temperature swing adsorption and their required regeneration temperatures [9] shown in Table 2-1.

Table 2-1: Solid sorbent DAC companies and their regeneration temperatures.

DAC Company	**Regeneration Temperature (°C)**
ClimeWorks	100
Global Thermostat	85-95
Antecy	80-100
Hydrocell	70-80

Solid sorbent DAC requires massive energy inputs at the commercial scale for the regeneration process. Because of these stipulations, finding an optimized solution to provide this energy requirement for DAC in both an economically effective and environmentally friendly way is vital to widespread adoption of the technology.

Cost-of-capture for DAC varies widely in literature. Chauvy et al. [2] outlined techno-economic analysis studies from literature on DAC technologies. Table 2-2 outlines the specific studies and scope of the work for the TEA.

Table 2-2: Summary of TEA studies for DAC technologies.

Author	Technical Aspects	Scope	Data	DAC Costs ($/t-$CO_2$)
Broehm et al [26]	Absorption vs. adsorption	Proposed TEA on DAC systems	Values from literature	$34-$468
Ishimoto et al [27]	Absorption and adsorption	Overview of DAC cost estimations	Values from literature	$850
Fasihi et al [9]	Focus on HT aqueous solution-based and LT solid sorbent-based	Literature review on DAC technologies and associated TEA	Values from literature and recalculated values	$38-$268
Kuru et al [28]	Solid sorbent DAC with geothermal	Geographical optimization of geothermal resources for DAC	Values from literature	$200-$1,040
McQueen et al [29]	Adsorption-based DAC technology	TEA of solvent DAC process coupled with energy system	Values from literature	$213-$587

These analyses guide cost estimates of different types of DAC, sorbent-based, energy-input based, and geographically based costs have been studied broken down in Table 2-2. The levelized cost of DAC has been debated in literature with values spanning over a large order of magnitude from \$30/t-CO_2 to \$1,100/t-CO_2 [2]. Wide variation in DAC costs lead to uncertainty on determining an accurate levelized cost of DAC value, making the goal of this study to highlight energy costs in a more flexible design framework. This study accommodates a range of assumptions about costs and efficiencies for DAC, without assigning a cost value on a DAC system.

2.2. Energy Sources to Meet DAC Energy Requirements

One challenge of adoption is finding economical renewable energy sources that maximize net-emissions captured and can consistently keep up with the demand to run DAC at a high-capacity factor. According to Breyer et al., overall heat demand is around 1,420-2,250 kWh_{th} of energy and in the range of 366-764 kWh_e needed to capture 1 tonne of CO_2 from ambient air in 2050 [10]. Brandani highlights the need for renewable energy sources for DAC [30]. He explains that these sources should be in excess or cannot be linked to the electrical grid for air capture

applications. He additionally explains the need for many massive installations and that policy makers need to base this analysis on reliable data for costs.

Researchers and companies have explored the thermal and economic constraints of using various energy sources for DAC. This includes natural gas [9], [31], [32], [33], solar photovoltaic (PV) [10], [34], [35], [36], battery storage [10], geothermal [28], [29], [33], [34], [37], [38], wind turbines [8], [10], [33], electric boilers [28], virtual power purchase agreements (VPPA) [17] and heat pumping [28], [32], [34], [35], [39]. Current literature shows that utilizing renewable forms of energy for the power requirements of DAC is beneficial on an economic basis due to the benefits of avoiding additional emissions from energy inputs to the system and mitigating the need for point source capture when using nonrenewable energy sources. Geothermal energy shows both thermal and economic opportunities for use with DAC. Pairing these technologies will be analyzed throughout the study and discussed in Section 2.4. with an analysis on current literature related to coupling geothermal with DAC.

2.3. Review of Geothermal Systems and Uses

Availability of geothermal resources is imperative for means of supplying energy for DAC. It provides a sustainable, low-carbon source of thermal energy that meets the requirements for DAC regeneration. Geothermal energy is one of the few renewable energy sources that offers a reliable and continuous energy supply, not needing to rely on storage or parasitic load profiles of other renewable technologies. In regions with abundant and accessible geothermal resources, utilizing this energy can make DAC more economically viable.

Snyder et al. [40] presented an analysis on geothermal resource availability specifically in Nevada and California. Monthly reports were generated at 19 power plants in California and Nevada covering 196 production wells and 175 injection wells. The average production

temperature was 151°C and the average injection temperature was 76°C for binary plants. The temperatures for the 196 production wells ranged from 75°C to 195°C for the plants. This study gives quantification to the availability of current geothermal production as well as opportunity with the widespread range of reservoir temperatures in the United States. Production and injection temperatures are also vital inputs to consider when designing a geothermal model.

Beckers et al. [12] presented an analysis on deep direct-use applications for geothermal in the United States. The study evaluated six U.S. Department of Energy funded university projects using geothermal energy for direct use applications. They calculated the base case levelized cost of heat values to be between $13-$350/MWh with the key drivers potentially lowering this levelized cost to be higher reservoir temperatures, lower drilling costs and lower discount rates. Economic incentives also would provide benefit to this cost value.

Many studies highlight geothermal energy as a viable renewable energy source for electricity generation [41], [42], [43], [44], [45], [46], [47], [48]. Geothermal energy is a sustainable and readily available source for electricity generation. Harnessing Earth's heat and utilizing an ORC to generate electricity from this high temperature source can be beneficial. However, using geothermal energy for direct use thermal applications, such as district heating or integration with DAC can be a more optimal use of the available enthalpy of the reservoir. Thermal energy applications have less energy conversion inefficiencies when compared to conversion to electricity, which is only about 12% efficient [11]. This study initially considered including comparisons with using geothermal energy for electricity generation for the grid, but it was excluded from the final scope due to anticipated decarbonization of the grid over the coming decades. Future work would benefit from a comparative analysis between using geothermal energy to generate electricity for the grid and using geothermal energy directly for DAC.

2.4. Review of Utilizing Geothermal Energy for DAC

Geothermal energy for DAC has been explored in literature, with different analyses contributing to understanding the basis of geothermal coupled with DAC. The literature explored in this section will highlight research papers that present geothermal energy as an applicable energy source for DAC heating and electricity requirements. These papers will highlight present research and the gaps that need to be addressed with further research and analyses.

Simon et al. [33] explored the levelized cost of carbon removal for both energy resources and for an air capture system. They used a sum of costs resulting from "generic" air capture devices. Energy resources considered include enhanced geothermal, natural gas combined cycle (NGCC), NGCC with 90% carbon capture and wind. Capital costs for these components are taken from available literature throughout the study. Additionally, the input parameters for the reference cases are composed of costs and efficiencies that authors estimate can be attainable for such devices and sources. The results of the study showed that high second law capture efficiencies and low-cost capture devices must be achieved to keep the cost of capture close to \$300/t-CO_2.

Kuru et al. [28] analyzed using geothermal resources to supply the thermal energy for solid sorbent DAC (S-DAC-GT) across various geographical regions. The authors analyzed regions that are favorable for S-DAC-GT including Texas Gulf Coast, Los Angeles Basin, Alaska's Cook Inlet, and Netherlands Groningen Gas Field. Unlike other studies primarily focused on energy sources and are region-agnostic, the paper includes regional insights and carbon intensities that pinpoint specific cases of the model. The analysis indicates a cost range of \$200-\$1,040/t-CO_2 removed, depending on the region. Energy requirements and associated costs were taken from the National Academies of Sciences, Engineering, and Medicine from 2019 [49]. The paper highlights that despite uncertainties in scaling DAC, geothermal energy reduces thermal energy costs by between

16-33% depending on the region, indicative of an economical solution to lower the cost of capture for DAC.

Ebrahimi et al. [34] presented a study that captures and liquefies CO_2 from power plant flue gases using an ejector refrigeration system, a Kalina power unit, and an organic Rankine cycle. The system is powered by thermal geothermal energy and PV for electricity, with a 97% thermal energy and 3% electrical energy split. The system produces 2.641 kg/s of liquid CO_2 with a heat pump COP of 3.661% and the ORC efficiency is 12.64%. Interestingly, the highest exergy destruction was from the PV cells, accounting for 39.81% of the total 24.2% reversibility. The authors concluded that an economic and environmental analysis with multi-objective optimization of the proposed system is recommended to further evaluate efficiencies of the integrated system, in addition to thermodynamic analyses.

Rosner et al. [38] explored using geothermal energy for DAC and suggested a cost of capture of \$100/tonne-CO_2. The study utilized conditions of a 195°C geothermal reservoir, 50 MW power plant and included the use of the 45Q tax credit in the analysis. Capital costs for the analysis are based on literature estimates. The authors analyzed scaling of DAC and its economic impact on the cost-of-capture. They investigated that at smaller scales, the cost-of-capture increases exponentially to about \$169/t-CO_2 at a 10 MW scale compared to \$85/t-CO_2 at a 100 MW scale. With the inclusion of the tax credit, they estimate that with DAC deployed at geothermal facilities in the United States, a net reduction of 270 million tonnes of CO_2 per year is possible by 2050.

Titus et al. [37] evaluated the techno-economic analysis of the performance of both geothermal-direct air carbon capture sequestration (DACCS) and geothermal bioenergy (BECCS). The cost analysis compared here utilized existing geothermal infrastructure to be retrofitted with CDR technologies. This approach lowered relative costs compared to traditional CDR methods.

The study compared geothermal-BECCS and geothermal-DACCS against conventional geothermal operations. The study found geothermal-BECCS to be more cost effective at $69/MWh (assuming a CO_2 market price of $100/tonne), specifically in geothermal retrofitting scenarios, compared to geothermal-DACCS at $143/MWh and traditional geothermal at $81/MWh. This is due to lower emissions abatement costs and increased electricity production, which improved overall efficiency. Geothermal-DACCS removed higher amounts of CO_2, although its parasitic energy load raised decarbonization costs. Because of this, geothermal-BECCS was more viable under these conditions.

McQueen et al. emphasized the need for DAC to prevent a 2°C temperature rise by 2100. They explain that DAC deployment is necessary and needs rapid deployment and technological advancements within the next decade for it to be a feasible option. The study highlights the high operational costs for DAC and outlines a roadmap to reduce DAC costs using low-temperature thermal energy in the form of geothermal. Transportation and storage are heavily analyzed in this study, resulting in a potential to deliver compressed, high purity CO_2 at a cost of < $300/t$CO_2$, with a scalable capacity of 19 $MtCO_2$/year. DAC system costs as well as energy input values and costs are from literature. An analysis of the 45Q tax credit is discussed and proves to be an economic incentive for these CDR technologies, informing economic viability of such systems for the future.

Simon et al., Kuru et al., Titus et al., and McQueen et al. utilized values from literature to guide the analysis for cost of CO_2 capture with DAC technologies. These analyses guide a starting point for understanding the economics behind using geothermal energy for supplying DAC energy requirements. Ebrahimi et al. study looked at a specific MEA based CO_2 capture cycle using geothermal heat for thermal requirements and photovoltaic electricity to fulfil electricity

requirements. This study focused on the thermodynamics of the coupled system for DAC, without use of a TEA. Finally, Rosner et al. evaluated the thermodynamics and economics of a dual-flash geothermal power plant with low temperature, low concentration solvent-based DAC. These results are based on a 195°C geothermal reservoir temperature and cost estimates are used from applicable published literature.

2.5. Research Needs for Geothermal-DAC Coupled Systems

The above literature review provides a summary of the current state of research for geothermal-DAC coupled systems. The review of existing studies confirms that DAC is expensive and is the core driver behind the need for further research and technological advancements. Current and future estimations of levelized cost estimates fall between \$245/tCO_2 and \$1,279/tCO_2 [9]. Table 2-3 breaks down papers that investigate the use of geothermal as energy input for DAC, and specifically the present economics of implementation.

Table 2-3: Summary of economic studies for geothermal-DAC technologies.

Author	Scope	Limitations
Simon et al [33]	TEA of wind, solar, geothermal, NGCC for DAC	Cost and energy estimates are literature-based Lacks thermal validation of coupled system
Kuru et al [28]	Geographical optimization of geothermal resources for solid-sorbent DAC using geothermal energy	Energy and capture costs are literature-based Lacks simulation validation
Ebrahimi et al [34]	Exergy utilization to capture CO_2 from power plant flue gas for liquification using geothermal heat and PV electricity	Doesn't incorporate economics Assumes a 97% thermal 3% electrical split
Rosner et al [38]	TEA for dual-flash geothermal power plant coupled with solvent-based DAC for 195°C reservoir	Cost values are literature-based No variation of reservoir or regeneration temperature
Titus et al [37]	Evaluating existing 275°C geothermal well infrastructure and transport costs for solid-sorbent DAC	Retrofit case with no variation of reservoir temperature Focuses on end-of-life CO_2 transport costs
McQueen et al [29]	TEA of solvent DAC process coupled with geothermal and nuclear energy	Cost and thermal estimates are literature based Focus on sequestration and storage of CO_2

Finding a low emission, inexpensive, readily available, and reliable source for providing energy to DAC is imperative to scientific research and future scaling of DAC including deployment. Literature confirms that utilizing a low-carbon, highly available source of geothermal

heat integrated with DAC plants can benefit net CO_2 removal [28], [33], [50], [51] and is widely researched, however these are high level studies that do not present a component-level thermodynamic model to validate cost and performance assumptions. This is a critical gap to address in literature because high-level models rely on significant assumptions about criteria including energy transfer, efficiency, and system performance, which has the potential to lead to misleading cost and performance estimations. Component-level validation would mitigate any risk with assumptions for heat exchanger effectiveness, turbine performance in the coupled system, or brine enthalpy performance.

Heavily debated economic evaluations throughout the literature have assessed the levelized cost of DAC systems assuming specific heat and electricity requirements from various energy sources, such as solar, wind, and geothermal [2], [9], [30], [31], [52], [53], [54], [55], [56], [57]. Yet, no studies review thermally validated models against other renewable energy sources in a direct comparison using the modeling outputs. This results in high-level evaluations that do not fully capture how energy is transferred or utilized within DAC coupled systems. Ebrahimi et al. did explore the use of geothermal for heat and PV for electricity, however the study lacks economic analysis of the simulation results. Comparing geothermal-DAC systems with other renewable energy inputs, along with associated costs is imperative. Whether from solar, wind, geothermal, etc., these alternatives have different efficiencies, capital costs, and availability factors to consider. Geothermal, for instance, offers a reliable, continuous heating source and can be integrated with DAC in a way that could reduce parasitic load. In contrast, wind and solar would require battery storage to account for load profiles. These stipulations are imperative to analyze in the techno-economic analysis when directly comparing these technologies.

Further, economic evaluations of geothermal-DAC coupled systems established a baseline for the levelized cost of such systems [29], [33], [34], [37], [38]. However, the studies utilize broad cost and performance assumptions without component-specific optimization, which could support the integration of such systems under varying reservoir temperatures or DAC regeneration temperatures. Rosner et al. presented a simulation-based model of a geothermal-DAC coupled system, however the cost estimates are literature-based and only one reservoir and regeneration temperature were used throughout the analysis. A component-level approach is essential for validating thermal performance under varying conditions including geothermal brine temperature, DAC regeneration temperature, and energy requirements of the geothermal-DAC coupled system. The cost of energy for DAC is highly dependent on these parameters, so understanding these systems at a granular level can provide accurate results for the performance of the complete system. Implementing accurate component-level values into a techno-economic analysis allows for a more reliable foundation when informing decision-making for DAC deployment.

2.6. Specific Aims of the Study

The literature review reveals a need for further investigation of thermodynamic modeling for how a geothermal system can be coupled with DAC with an emphasis on optimizing cycle design for maximized efficiency and to size components to be costed and implemented into a techno-economic analysis. The analysis presented here enhances understanding of DAC feasibility by utilizing a component-level thermodynamic model specifically refined for a geothermal-DAC coupled system. Each individual component is optimized for various reservoir conditions, regeneration temperatures, and configurations in all scenarios. This comprehensive thermodynamic and economic analysis is compared against other renewable energy sources to

establish a selection criteria framework based on resource availability in diverse geographical regions.

CHAPTER 3. Modeling Approach

3.1. Geothermal + DAC Coupled Systems

A geothermal-DAC coupled system was optimized to maximize efficiency of electricity generated by the ORC. This involved precise adjustments to operating conditions, including flow rates, temperatures, and pressures to meet process requirements. The system was modeled, optimized, and thermodynamically validated in ASPEN Plus, followed by an economic analysis to determine favorable configurations under various conditions. Heat utilization of geothermal brine was validated across reservoir temperatures, DAC regeneration temperatures and configurations (split stream DAC vs. heat integrated DAC). Assessing split-stream and parallel configurations has implications on both energy efficiency and economic performance of the coupled system. In split-stream, there is a higher initial temperature of the brine to the ORC. The DAC can access the higher-temperature brine to improve regeneration efficiency of the sorbent being used. This also allows the split stream to be a driving input to the model, giving better optimization procedures of the flow rate of the ORC along with the evaporator outlet pressure. The DAC heating process also isn't completely reliant on a single stream. For the series case, by sending brine through the ORC, it allows the system to extract as much thermal energy as needed for power generation before sending the lower exergy portion to supply the heating requirement especially when the regeneration temperature is low. Figure 3-1 illustrates how DAC can be integrated with geothermal systems.

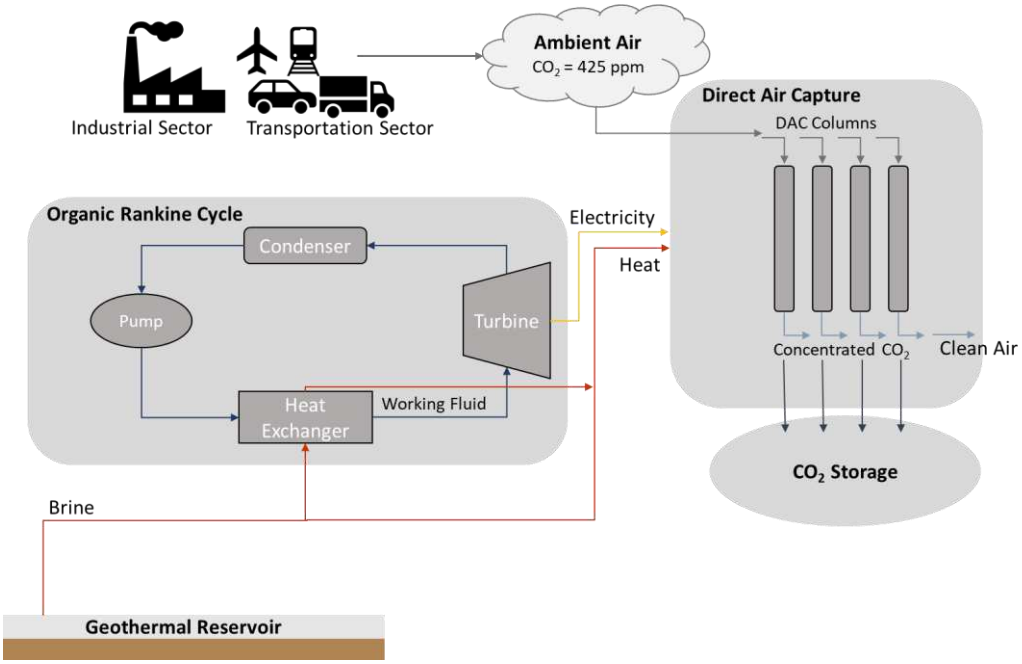

Figure 3-1: System diagram of geothermal reservoir coupled with DAC in parallel and series heat integration.

The geothermal-DAC integrated system utilizes an ORC to convert thermal energy from the brine into electricity — essential for various DAC processes including operation of blowers, pumps, compressors, and auxiliary equipment [57]. The high-temperature geothermal brine meets 80% of the energy demand for the DAC process as heat, while the ORC generates the remaining 20% electricity required. The brine is either split to fulfill the heating and electricity needs in a 4:1 ratio in parallel split-stream or supplies heat to the ORC evaporator and then to the DAC system in series heat-integrated configurations.

Within the ORC, the working fluid is heated by geothermal brine in the evaporator. As the fluid absorbs heat, its temperature rises until it reaches its boiling point, and then undergoes a phase change from liquid to vapor. The high-pressure vapor drives a turbine, where its expansion rotates the turbine blades to generate electricity. After expansion, the low-pressure vapor enters the condenser where it releases latent heat to the cooling water and condenses back into a liquid state.

The condensed working fluid is pressurized by a pump and recirculated into the evaporator, completing the closed loop cycle.

The electricity produced by the ORC powers the DAC auxiliaries, while the direct heat from the brine satisfies the DAC's heating requirements. This process enables the DAC columns to strip CO_2 from ambient air, releasing pure air back into the atmosphere while capturing the concentrated CO_2 for underground storage or commercial utilization.

3.2. Thermodynamic Model

A thermodynamic model was developed in ASPEN Plus to represent the performance of the Geothermal+ORC system. To initialize the model in each case, an approximation method was used to establish initial guesses for the key inputs. First, the available duty for DAC was estimated by accounting for the expected isentropic efficiency of the ORC, while adhering to the 4:1 ratio of thermal power and electrical work generated. The total estimated duty available in the brine is calculated using Equation 1.

$$Q_B = \dot{m} \times C_P \times (T_H - T_C) \tag{1}$$

65% of the Carnot efficiency [58] was assumed to predict the actual isentropic efficiency of the ORC. A specific isentropic efficiency was calculated for each comparative geothermal-DAC case depending on reservoir temperature and regeneration temperature, rejecting to ambient. Using this predictive value, the relationship between the W_{Turb} and Q_{DAC} values are represented in Equations 2 and 3 respectively.

The relationship between Q_{DAC}, Q_B, W_{Turb}, and η_{ORC} is shown in Equation 2:

$$Q_{DAC} = Q_B - \frac{W_{Turb}}{\eta_{ORC}} \tag{2}$$

W_{Turb} was calculated using Equation 3 to maintain the 4:1 constraint on the heating and work of the system:

$$Q_{DAC} = \frac{1}{4} \times W_{Turb} \tag{3}$$

Finally, the split fraction for the parallel case was calculated using Equation 4.

$$Split\ Frac. = \frac{Q_{DAC}}{Q_B} \times \frac{T_{Res} - T_{Reinj}}{T_{Res} - T_{DAC}} \tag{4}$$

The split fraction was set into the splitter block in the ASPEN model to initialize the manual optimization. The DAC heater unit output a specific heat duty along with the turbine work produced at this calculated split fraction. In most cases, the cycle could not achieve 65% of Carnot. Therefore, the split fraction had to be meticulously decreased, noting the relationship between the DAC heat duty and turbine work produced after each adjustment. The constraint on these values needs to maintain a 4:1 ratio, necessary for the DAC system energy requirements. The ORC working fluid flow rate meticulously increased while the split fraction was meticulously decreased until the DAC heat duty and turbine work were at a 4:1 ratio. From here, the model could be further optimized by increasing the evaporator outlet pressure at these conditions to pull additional work from the turbine without crossing the minimum temperature approach constraint of the evaporator of 2°C and thus avoiding temperature cross. Once this outlet pressure value was maximized, the split fraction could be increased slightly, increasing the DAC heat duty each time, and again, the ORC working fluid could be increased improving the turbine work generation. Throughout this process, the driving constraint is the 4:1 ratio for the DAC heater and turbine work produced. This process continued until the maximum DAC heat duty was achieved while the turbine simultaneously produced ¼ of that heating duty. Once those values are maximized as indicated by diminishing returns on further adjustments, the optimization is considered completed.

Table 3-1 shows specific outputs to understand the specific value changes during the optimization process from calculated data points to the optimized data points. The heat utilization of the available brine changes during each step until the system is optimized adhering to the 4:1 DAC energy constraint.

Table 3-1: ASPEN model before and after optimization for 205°C reservoir and 80°C regeneration.

Optimization Step	Split Fraction	WF Flow Rate (kg/s)	Evaporator Outlet Pressure (bar)	DAC Heat Duty (kW)	Turbine Work (kW)
1. Calculated Values	0.4666	-	-	84300	21080
2. Initial Outputs	0.4666	138	10	84560	16490
3. Lower Split Fraction	0.3837	161	10	69530	16940
4. Optimized Outputs	0.3837	161	13	69530	18730

Figure 3-2 presents T-Q curves for the outputs in Table 3-1 to better highlight the heat utilization shifts in ASPEN and how the brine heat is distributed during the optimization process.

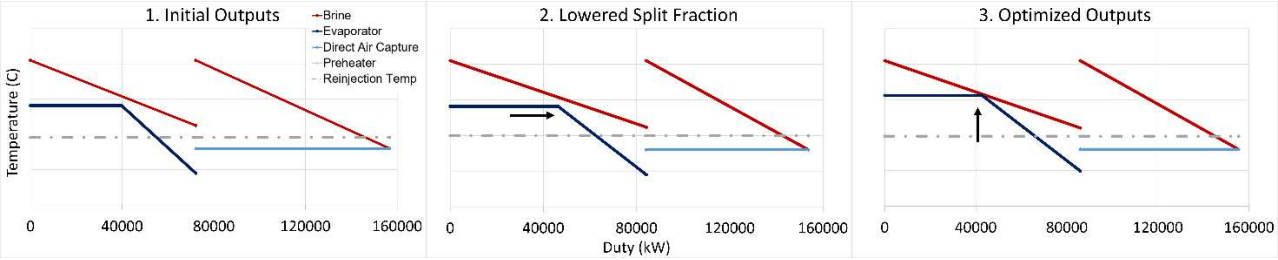

Figure 3-2: Temperature vs. heat duty curves for 205°C reservoir and 80°C regeneration temperatures showing the ASPEN optimization process.

In Step 1, the ORC side has a large temperature gap between the brine and the ORC working fluid, leading to unutilized thermal potential. These results are derived from the initial calculated values, assuming 65% of Carnot. The ORC cannot achieve that efficiency value so an

optimization process must be used to meet DAC energy requirements while effectively distributing the available brine enthalpy. In Step 2, the split fraction of brine to the DAC heater is lowered, supplying more of the available brine heat to the ORC. This slightly improves the system performance, by providing more exergy to the system for the turbine to produce work. Finally in Step 3, there is a vertical shift in the ORC side of the evaporator. The system is better matched to the heat source, minimizing potential thermal losses, and improving overall system performance. The brine is utilized most effectively, capitalizing on all available heat for DAC while meeting 4:1 energy requirement and while avoiding temperature cross in the evaporator. A similar process was used in the series case; however, the outlet temperature of the evaporator was the driving predictive value for the efficiency of the ORC. 65% of Carnot was assumed and using the same process in Equations 1-3, the outlet temperature of the evaporator was calculated as an initial guess for the system. The same manual optimization process as the parallel case was performed, however, the outlet temperature was the driving value changed while optimizing the system performance.

Important to note is that as reservoir temperatures increase, the isentropic efficiency increases due to having more available enthalpy from the brine, under the same mass flow rate entering the system. Additionally, at lower DAC regeneration temperatures, the isentropic efficiency is typically higher as the DAC system is more efficient. As DAC regeneration temperatures increase, there is a noticeable drop in isentropic efficiency. This is due to less of the available geothermal energy effectively converted into useful work.

Figure 3-3 shows a representative stream table of a case model's respective inputs and outputs for both the series and parallel cases.

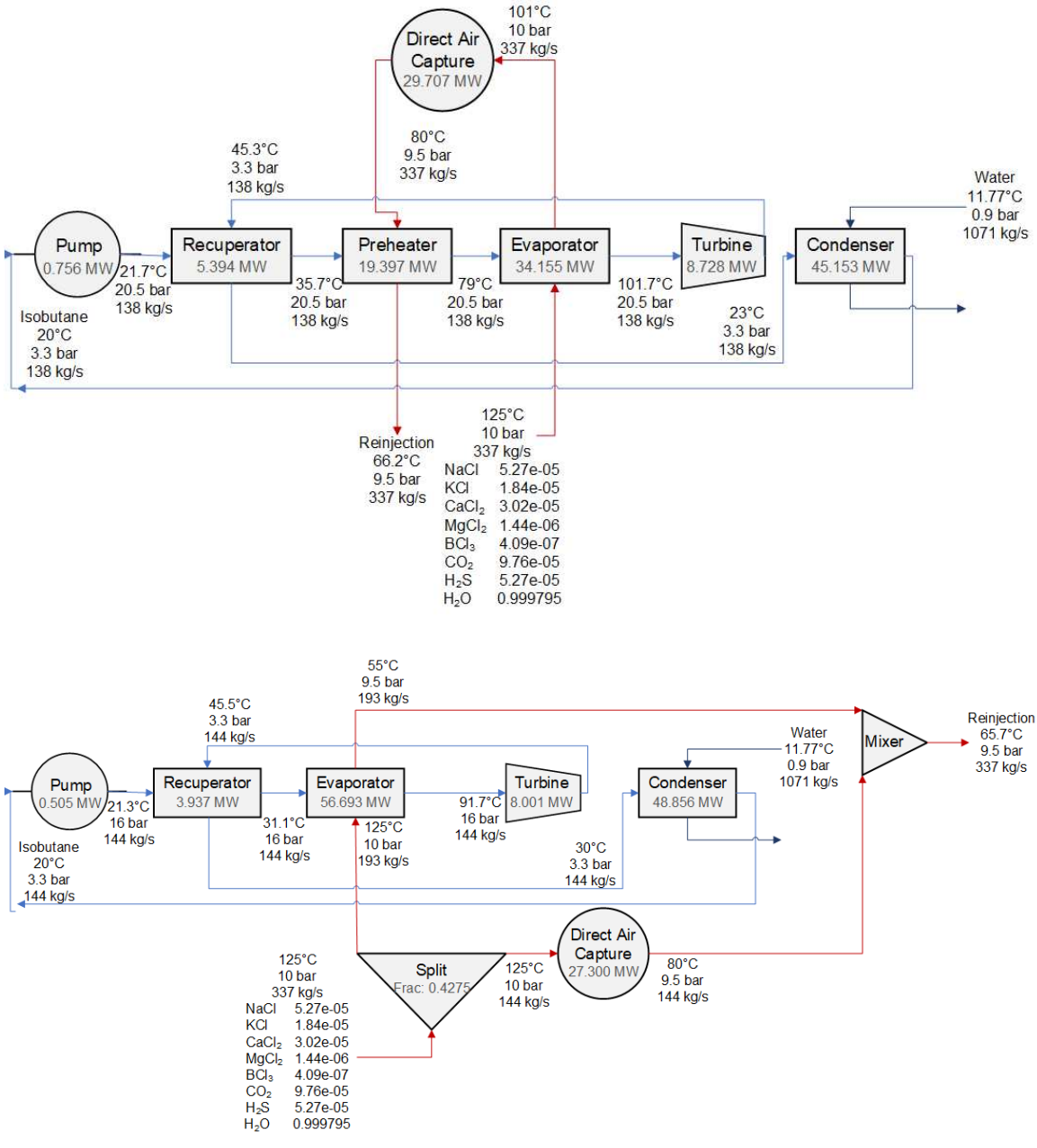

Figure 3-3: Stream table for 125°C geothermal reservoir and 80°C regeneration temperature for **(A)** series case and **(B)** parallel case.

Figure 3-4 shows the ASPEN Plus model for the geothermal-DAC integrated system. Cases shown below are for the 125°C parallel case (A) and series case (B) with 80°C regeneration temperature. Input and output values for temperature, pressure, mass flow, heat duty, and power are shown throughout the streams. For the series case with a 125°C reservoir and 120°C

regeneration temperature, the DAC unit is placed before the ORC evaporator due to the small temperature gradient. Because of that, the geothermal brine flows directly to DAC and then into the ORC.

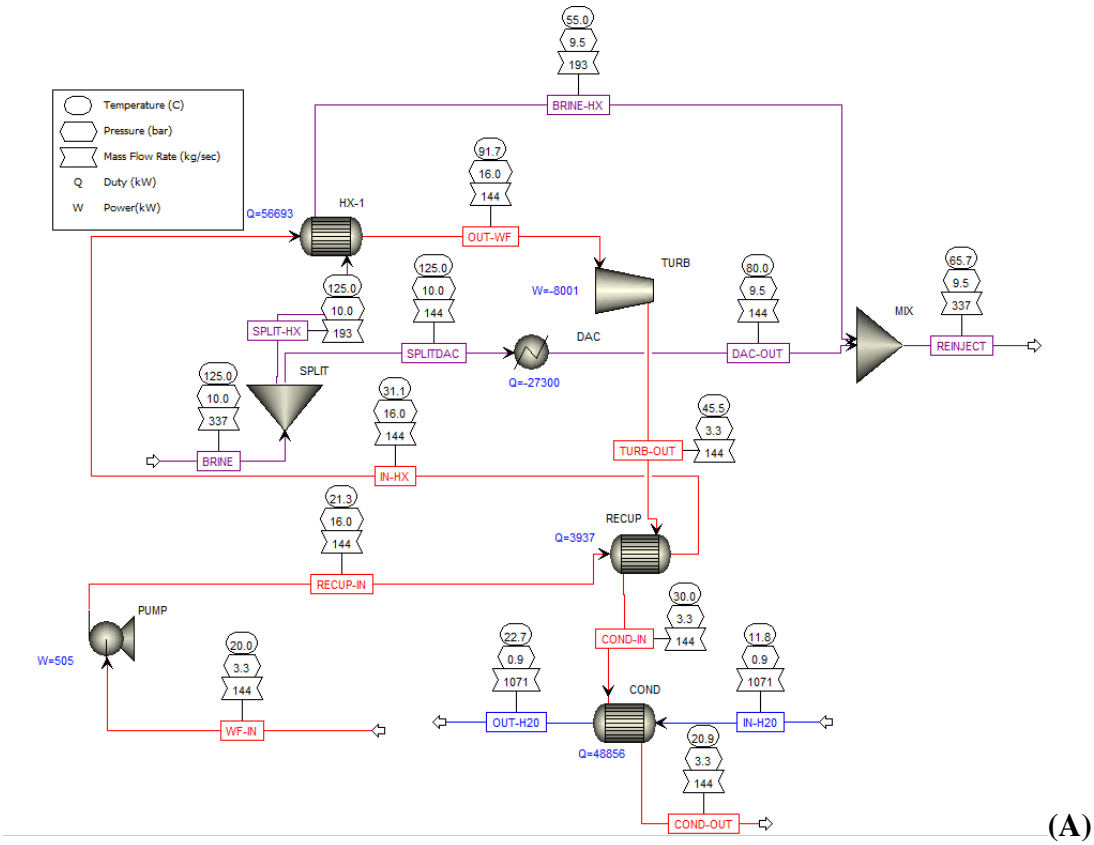

(A)

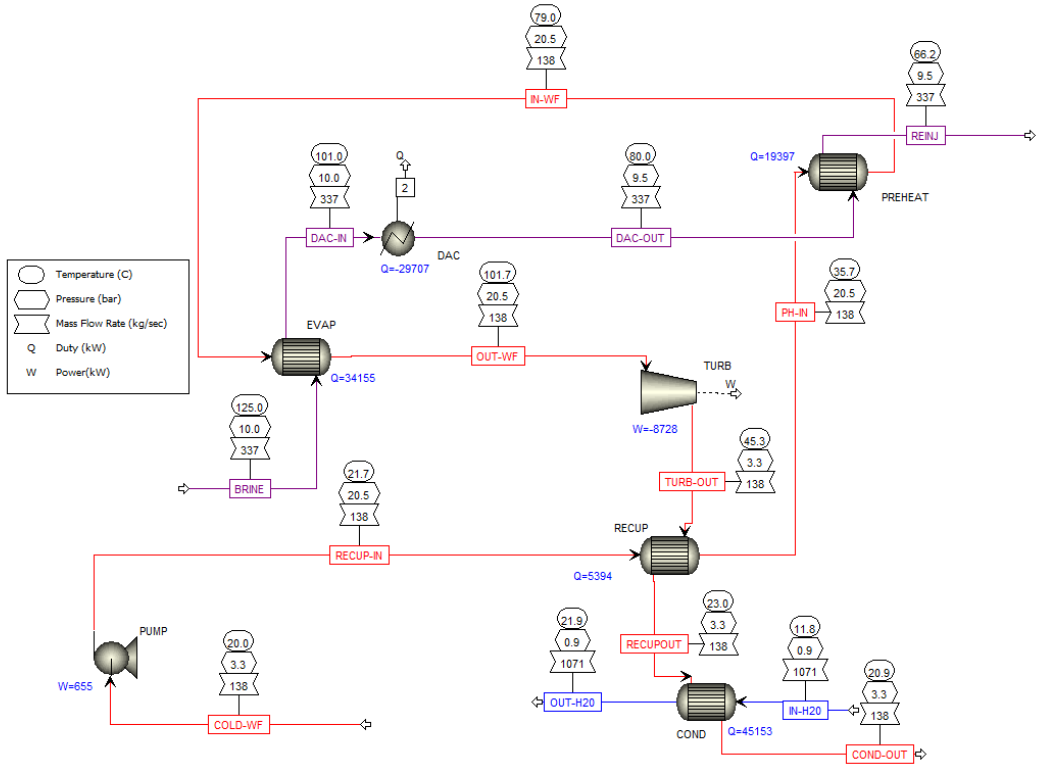

(B)

Figure 3-4: ASPEN Plus software diagram with inputs and outputs for 125°C reservoir temperature and 80°C regeneration case **(A)** parallel case and **(B)** series case.

The block types in the ASPEN model are subject to specific constraints designed to optimize system performance within the cycle. The pump operates under a discharge pressure constraint and is assigned an isentropic efficiency of 65%. The recuperator is configured with a hot stream outlet temperature constraint, countercurrent flow direction, and calculated U-value. The preheater is constrained to achieve a cold stream outlet temperature approximately 1°C below DAC regeneration temperature, ensuring the working fluid is preheated to the highest possible temperature before entering the evaporator. The preheater was optimal in this location due to the DAC regeneration temperature set higher than the reinjection temperature. Extracting additional enthalpy from the brine and preheating it before the evaporator makes the ORC more efficient. In the evaporator, a 3°C cold stream outlet superheat constraint is maintained in all cases and the heat

exchangers are constrained as two-phase with a 2°C minimum temperature approach. In the parallel case, the split fraction is adjusted as an input, while in the series case, the hot stream outlet temperature is calculated and adjusted as well. The cold side outlet pressure is maximized until the fluid is fully vaporized ensuring maximum absorption of heat energy before the working fluid flows to the turbine. The turbine operates with an 85% isentropic efficiency and a discharge pressure constraint to maintain an optimal condensing state. The condenser block receives cooling water on the cold side at a constant temperature, pressure, and flow rate, cooling the working fluid passing through the hot side. The condenser maintains a 2°C outlet of subcooling on the hot side, ensuring the working fluid condenses fully into a liquid state before re-entering the pump to complete the cycle.

After initial guesses were calculated from the equations in Section 3-2, the ASPEN model was manually optimized to generate the most heat duty from the DAC heater unit given the initial conditions. The inputs and assumptions for the model are outlined in Table 3-2.

Table 3-2: ASPEN Plus model and inputs for the coupled system.

Variable	**Value**	**Units**	**References**
Pump Efficiency	65	%	[59]
Evaporator Cold Stream Degree Superheat	3	°C	[60]
Evaporator Constant U	62.5	Btu/hr-sqft-°F	[61]
Evaporator Minimum Temperature Approach	2	°C	[62]
Turbine Isentropic Efficiency	85	%	[11]
Geothermal Brine Flow Rate	336.95	°C	[63]
Reinjection Temperature, T_{REINJ}	>65	°C	[64]
Cooling Tower Water Temperature, T_{CW}	11.77	°C	[65]
Cooling Tower Water Flow Rate, $\dot{m}_{CW}$	1071	kg/s	[66]
Cooling Tower Power	19.2	kW/400 tons	[67]
Geothermal Brine Temperature	125-205	°C	[68]
DAC Regeneration Temperature	80, 100, 120	°C	[4], [9], [25]
DAC Heat Duty:Turbine Work Ratio	4:1	kW_{th}:kW_e	[9], [10]

The DAC heat duty was calculated to estimate what the system could extract from the brine enthalpy given reservoir temperature and DAC regeneration temperature. The working fluid

temperature into the pump of the ORC was 20°C. The evaporator was constrained to provide 3°C cold stream of superheat with a constant U value of 62.5 btu/hr-sqft-°F, validated by Perry's Chemical Engineering [61]. The brine from the geothermal reservoir was held at a constant mass flow rate to create a fair comparison of available heat across configurations at 336.95 kg/s. The brine used was 1% salinity. Other significant assumptions were restricting the reinjection temperature of the brine to being higher than 65°C to avoid too low of temperatures reinjected back into the reservoir along with keeping the cooling tower temperature and flow rate the same throughout at 11.77°C and 1,071 kg/s respectively. The model is not sensitive to pressure drops in the liquid-only system so inputs for pressure were arbitrary.

Current geothermal plants use 1% salinity brine to avoid scaling and fouling in the heat exchangers and piping [69]. This scaling would reduce the heat transfer efficiency and would require frequent cleaning, increasing operating costs and downtime of the system. This brine salinity is held constant throughout the ASPEN modeling and its chemical composition is shown in Table 3-3. These ion/metal concentration values are taken from the Salton Sea geothermal power plant [70].

Table 3-3: Geothermal brine 1% salinity chemical composition.

Chemical Compound	**Mole Fraction**
NaCl	0.00516667
KCl	0.0018
$CaCl_2$	0.00295833
$MgCl_2$	0.00014083
BCl_3	0.0000401
CO_2	0.00957
H_2S	0.000429
Water	97.9885067

The working fluid used in the analysis was changed depending on reservoir temperature, as another sensitivity parameter for the study to understand working fluid performance in an ORC. Table 3-4 outlines the working fluid used respective to each reservoir temperature.

Table 3-4: Working fluid table used for each reservoir temperature.

Reservoir Temperature (°C)	Working Fluid
125	Isobutane
145	n-Butane
165	n-Pentane
185	Isopentane
205	Cyclopentane

3.3. Optimization of ASPEN Model Inputs

The inputs were adjusted throughout the analysis to create an optimized geothermal-DAC thermodynamic system as discussed in Section 3.2. Inputs were adjusted accordingly to create a best case of CO_2 removal per scenario. The pump inlet pressure was adjusted based on the working fluid being used. Using a T-s curve in Engineering Equation Solver (EES), the minimum allowable pressure was determined for each working fluid and temperature profile to prevent condensation within the turbine during expansion. The working fluid flow rate was adjusted simultaneously with the evaporator outlet pressure, meticulously increasing, and decreasing each value by one unit against the original approximation until the highest DAC heating value was achieved. These adjustments maximize turbine power output constrained in the 4:1 ratio, enabling the highest CO_2 removal per configuration.

As shown in Table 3-2, the geothermal brine was evaluated within a range of 125°C to 205°C, with increments of 20°C to represent variability in geothermal resource availability across both

current and potential future reservoirs. The lower bound of 125°C was selected as the minimum viable temperature for DAC regeneration, aligning with the 120°C upper limit for effective regeneration and thermal efficiency of the ORC. The upper bound of 205°C corresponds to the maximum reservoir temperature accessible without the need for EGS. The DAC regeneration temperature varied between 80°C and 120°C, also with 20°C increments. Two configurations were tested: DAC in series and DAC in parallel, resulting in a set of 30 test conditions for performance evaluation.

3.4. Economic Model

A discounted cash flow (DCF) model was developed to evaluate the economic viability of renewable energy cases for DAC by estimating cash flows and accounting for technological constraints when projected out 30 years. Capital costs for the ORC are used from ASPEN Plus Process Economic Analyzer. Capital expenditure (CAPEX) and other associated costs are taken from the EIA "Capital Costs and Performance Characteristic Estimates for Utility Scale Electric Power Generating Technologies" report [15], in addition to operational expenditure (OPEX) costs associated with running and upkeep of the system. All cost values assume a new build for technologies, including geothermal power plants, solar PV arrays and batteries for storage. Values for the analysis were scaled according to power requirements needed in each case.

CAPEX for the geothermal power plant is broken down into categories outlined in Figure 4-4. OPEX categories for geothermal include labor, turbine maintenance, materials and contract services, and administrative costs. OPEX categories for solar and batteries includes module cleaning, inverter maintenance, battery maintenance, 10-year battery replacements, and preventative maintenance. Land costs and acreage requirements are calculated based on estimates from EIA and included in the cost analysis [15]. CAPEX and OPEX estimates for solar and

batteries systems associated with the Solar+Battery and Geothermal+Firm Renewables cases were scaled to match the electricity requirements of the DAC system, ensuring a consistent capacity with costs associated for a comparative analysis.

The analysis incorporated specific CAPEX and OPEX costs based on distinct components and configurations. The ORC capital costs for the configurations utilizing geothermal energy to meet electricity requirements of DAC were calculated using ASPEN Plus. Equipment cost for the evaporator, recuperator, preheater, condenser, and pump were sized according to the system requirements within each model as reservoir and regeneration temperatures change. The turbine cost was estimated based on the specific power output of each configuration, ensuring accuracy by directly linking component costs to respective thermodynamic performance. This offers a more precise cost estimation compared to EIA data, which lacks integration with thermodynamic sizing. The techno-economic analysis incorporates these detailed capital costs, while drilling, exploration, well, maintenance costs, etc. are adopted from the EIA report as broader infrastructure components. To validate the use of ASPEN data in this analysis, a comparison between EIA and ASPEN data presented a $/kW value for CAPEX of the geothermal-ORC system. EIA cost was calculated at $1,174.46/kW and ASPEN Plus was $1,002.95/kW under the same operating conditions. This justified the use of ASPEN data for the analysis.

In scenarios where geothermal resources supplied heat exclusively to the DAC system and electricity was sourced externally, the costs associated with ORC components were excluded. The grid emissions factor (EF) for the grid electricity case was 460 gCO_2/kWh [71]. The inputs utilized in the DCF models are detailed in Table 3-5.

Table 3-5: Economic discounted cash flow model assumptions.

Variable	Value	Units	Reference
Loan Equity	40	%	[72]

Loan Interest	8	%	[72]
Loan Term	25	Years	[72]
Depreciation Modified Accelerated Cost Recovery System	7	Years	[72]
Construction Period	3	Years	[72]
Tax Rate	35	%	[72]
Discount Rate	10	%	[72]
Discounted Cash Flow Projection	30	Years	[72]

3.4.1. Levelized Cost of Energy

Assumed economic conditions are held constant throughout all scenarios for a direct comparison between technologies. In addition, the systems are all scaled to a 30-year lifetime. The levelized cost of energy (LCOE) for DAC is calculated using Equation 5 to provide a direct comparison between scenarios.

$$LCOE = \frac{\sum_{t=1}^{n} \frac{A_t}{(1+i)^t}}{\sum_{t=1}^{n} \frac{M_{t,CO_2}}{(1+i)^t}} \quad (5)$$

Levelized cost of DAC has been debated in literature with values spanning over a large order of magnitude from $30 and $1,100 [2] per tonne of CO_2, as discussed in Chapter 2. The goal of this study is to highlight energy costs in a more flexible design framework to accommodate a range of assumptions about costs and efficiencies for DAC. A unanimous stand-in levelized cost of DAC could not be determined from literature, therefore, the cost values presented are the levelized cost of energy input for DAC. This value includes all CAPEX and OPEX costs associated with the energy input for a DAC plant to run at full capacity.

3.5. Sensitivity Analysis

A sensitivity analysis was included to account for variability in the results, providing a comprehensive assessment of geothermal potential across different global contexts based on resource availability. Additionally, the performance of different working fluids within the ORC

was assessed to understand their relative efficiencies. The two different configurations, parallel and series, were evaluated to identify the optimal placement of DAC within an integrated system, with the most effective configuration result presented when not specified. Furthermore, a range of DAC regeneration temperature was examined, from lower temperatures of 80°C to the higher temperatures currently used of 120°C.

CHAPTER 4. Results and Discussion

To evaluate integrating geothermal energy with DAC, 30 distinct scenarios were modeled and optimized using ASPEN Plus. Configurations are broken down in Table 4-1, showing the different reservoir temperatures, DAC placement, and DAC regeneration temperatures.

Table 4-1: Configurations for thermodynamic ASPEN Plus modeling.

Reservoir Temperature (°C)	**DAC Regeneration Temperature (°C)**	**Configuration**
125	80	Parallel (Split-Stream)
145	100	Series (Heat-Integrated)
165	120	
185		
205		

Table 4-2 presents the raw data tables for key metrics of geothermal-DAC coupled systems for the configurations tested. The table highlights critical thermodynamic outputs such as DAC heat duty, turbine work, evaporator, and recuperator heat flows, and required cooling tower power for the ORC working fluid. Economic outputs including ORC capital cost and cost of power are inputs to the technoeconomic analysis, along with various environmental impact metrics such as CO_2 removed annually. This table presents the raw data to understand performance trade-offs that guide the technoeconomic analysis outputs and is crucial for comparing the efficacy of different system configurations under variable operating conditions.

Table 4-2: Raw data and calculated values for ASPEN Plus modeling **(A)** parallel configuration and **(B)** series configuration. The inputs are direct inputs for the ASPEN model, outputs are the ASPEN model outputs for each case showing the various component performance, and the calculated values are post processed data used to inform the TEA.

(A)

Case		ASPEN Inputs						
Brine Temp	**DAC Regeneration Temp (°C)**	**Working Fluid**	**ORC WF Flow Rate (kg/s)**	**Brine Pressure (bar)**	**Calculated Split Fraction**	**Evaporator Outlet Pressure (bar)**	**Actual Split Fraction**	**ORC WF Low Pressure (bar)**
125	80	Isobutane	144	10	0.4591	16	0.4275	3.3
	100	Isobutane	116	10	0.7385	14.5	0.5635	3.3
	120	Isobutane	53	10	3.200	9	0.8410	3.3
145	80	n-Butane	144	10	0.4503	18	0.4070	2.4
	100	n-Butane	135	10	0.5833	15	0.5080	2.4
	120	n-Butane	115	10	0.9135	10	0.5750	2.4
165	80	n-Pentane	136	10	0.4528	15	0.3607	0.8
	100	n-Pentane	132	10	0.5325	11	0.4365	0.8
	120	n-Pentane	118	10	0.6716	9	0.5341	0.8
185	80	Isopentane	170	20	0.4590	19	0.4050	1
	100	Isopentane	180	20	0.5114	14	0.4680	1
	120	Isopentane	165	20	0.5857	12	0.5399	1
205	80	Cyclopentane	161	20	0.4666	14	0.3837	0.5
	100	Cyclopentane	151	20	0.5022	13	0.4295	0.5
	120	Cyclopentane	143	20	0.5449	12	0.4810	0.5

Case			ASPEN Outputs					
Brine Temp	**DAC Regeneration Temp (°C)**	**DAC Duty (kW)**	**Turbine Work (kW)**	**Evaporator Duty (kW)**	**Recuperator Duty (kW)**	**Condenser Duty (kW)**	**Pump Work (kW)**	**Reinjection Temp (°C)**
125	80	27300	8001	56693	3937	48856	505	65.55
	100	20385	5983	45176	2768	39357	355	79.02
	120	6016	1846	19870	669	17982	83	106.84
145	80	37689	10737	64339	6212	53233	596	73.31
	100	32680	9333	59730	4844	50437	455	80.14
	120	20640	5975	49027	2978	42512	232	96.23
165	80	43894	11990	63869	11617	49787	340	89.86
	100	40777	11155	61540	10673	48323	298	93.68
	120	34708	9498	54569	8961	43198	237	102.91
185	80	61206	16867	77648	17602	59299	756	88.88
	100	57502	15807	80385	15891	62787	578	89.56
	120	50994	14031	72693	13311	57555	489	96.46
205	80	69533	18762	89607	6169	68596	447	93.79
	100	65696	17564	75841	4878	58371	352	100.39
	120	59905	16144	78703	4684	60927	338	110.11

Case		Calculated Values				
Brine Temp	**DAC Regeneration Temp (°C)**	**Isentropic Efficiency**	**ORC Capital Cost ASPEN ($)**	**Cost of Power ($/kW)**	**Cooling Tower Power (kW)**	**CO_2 Removed (t-CO_2/year)**
125	80	0.1462	1,0286,235	1,504.69	660	135,879.5
	100	0.0953	7,945,025	1,558.94	532	101,461.7
	120	0.0233	4,107,900	2,702.34	243	29,943.3
145	80	0.1477	11,408,945	1,210.88	719	187,588.4
	100	0.1192	10,653,105	1,299.67	681	162,657.3
	120	0.0651	7,388,155	1,429.37	574	102,730.9
165	80	0.1241	9,943,100	905.77	672	218,472.4
	100	0.1116	9,497,685	930.75	653	202,958.3
	120	0.0891	8,364,240	963.89	583	172,751.2
185	80	0.1592	14,619,575	954.90	801	304,639.0
	100	0.1434	13,945,195	969.70	848	286,203.1

	120	0.1196	12,833,865	1,005.42	777	253,811.0
205	80	0.1474	13,678,610	786.65	926	346,084.7
	100	0.1330	13,018,640	792.68	788	326,986.9
	120	0.1172	11,735,490	783.25	823	298,163.5

(B)

Case		**ASPEN Inputs**						
Brine Temp	**DAC Regeneration Temp (°C)**	**Working Fluid**	**ORC WF Flow Rate (kg/s)**	**Evaporator Outlet Temperature (°C)**	**Evaporator Outlet Pressure (bar)**	**Brine Pressure (bar)**	**ORC WF Low pressure (bar)**	**Recuperator Hot Stream Outlet Temperature (°C)**
125	80	Isobutane	138	101	20.5	10	3.3	23
	100	Isobutane	95	115	20	10	3.3	23
	120	Isobutane	35	110	18	10	3.3	23
145	80	n-Butane	158	117	18.75	10	2.4	29
	100	n-Butane	123	124	20	10	2.4	29
	120	n-Butane	74	133	18	10	2.4	29
165	80	n-Pentane	166	118	13	10	0.8	33
	100	n-Pentane	133	132	14.5	10	0.8	33
	120	n-Pentane	94	145	16.5	10	0.8	34.5
185	80	Isopentane	203	128	21	20	1	29
	100	Isopentane	168	144	21	20	1	30
	120	Isopentane	145	155	21	20	1	29
205	80	Cyclopentane	188	142	17.75	20	0.5	31
	100	Cyclopentane	162	156	20	20	0.5	31
	120	Cyclopentane	138	168	21	20	0.5	31

Case		**ASPEN Outputs**						
Brine Temp	**DAC Regeneration Temp (°C)**	**Preheater Cold Outlet (°C)**	**DAC Duty (kW)**	**Turbine Work (kW)**	**Evaporator Duty (kW)**	**Preheater Duty (kW)**	**Condenser Duty (kW)**	**Pump Work (kW)**
125	80	79	29702	8729	34158	19395	45153	655
	100	99	19895	5928	15693	21105	31084	438
	120	59	7154	2131	11385	2138	11452	142
145	80	41 (increase)	42074	12026	50177	19644	58131	686
	100	99	34158	9748	30172	25115	45738	578
	120	100	18615	5448	17281	15584	27226	306
165	80	79	53865	14894	67825	11109	60191	493
	100	99	45614	12520	47804	15975	48225	444
	120	119	35896	9949	29088	17328	35564	363
185	80	79	71018	19905	80375	8823	76791	964
	100	99	62886	17352	60235	16816	58319	831
	120	119	53301	14841	41386	24981	50335	717
205	80	79	89714	24175	91771	10859	76532	667
	100	99	80280	21677	72933	16273	65948	649
	120	119	69384	18712	55395	20814	56178	581

Case		**Calculated Values**					
Brine Temp	**DAC Regeneration Temp (°C)**	**Reinjection Temp (°C)**	**Cooling Tower Power (kW)**	**Carnot Efficiency**	**ORC Capital Cost ASPEN ($)**	**Cost of Power ($/kW)**	**CO_2 Removed (t-CO_2/year)**
125	80	66.2	610	0.1685	13,053,685	1,748.85	147835.0
	100	85.1	420	0.0941	8,794,500	1,734.56	99022.8
	120	110.5	155	0.0273	4,733,745	2,580.65	35607.4
145	80	65.8	785	0.1781	15,733,050	1,490.60	209413.8
	100	82.2	618	0.1272	12,273,560	1,435.13	170013.7

	120	109.1	368	0.0581	6,942,110	1,454.07	92651.9
165	80	72.1	813	0.1753	13,450,230	989.86	268100.8
	100	88.7	651	0.1325	11,698,130	1,023.94	227033.3
	120	107.8	480	0.0950	10,310,505	1,132.32	178664.2
185	80	73.7	1037	0.2121	19,576,475	1,093.42	353476.0
	100	87.9	788	0.1668	16,211,300	1,030.38	313000.8
	120	102.4	680	0.1301	13,596,125	1,011.30	265293.6
205	80	72.3	1034	0.2288	20,379,925	906.81	446531.0
	100	88.5	891	0.1874	17,459,735	867.04	399575.5
	120	105.4	759	0.1468	15,131,310	871.01	345343.1

The cooling tower power required for the ORC working fluid was calculated using Equation 6, assuming power requirements from the SPX Cooling Technologies, Inc. report on Cooling Tower Energy [73].

$$\dot{W}_{CW} = 0.0135 \times Q_{Cond} \tag{6}$$

Cost of power is calculated using Equation 7.

$$\dot{W}_{Cost} = \frac{Cost_{ORC}}{W_{Net}} \tag{7}$$

4.1. Brine Exergy Performance

Figure 4-1 presents T-Q curves for 4 representative scenarios, illustrating two different reservoir temperatures and the two configurations. The series configuration demonstrated overall superior performance when coupled with DAC. These diagrams highlight the challenges in extracting enthalpy from the brine, particularly in the parallel case. Rather than a global optimum for best possible system, we consider these results to be a good estimation of the optimum without changing the system configuration by adding more equipment, like additional heat exchangers or multiple turbines. Additionally, these graphs support that the model obeys the first and second laws of thermodynamics throughout the power cycle, confirming that the energy remains balanced, and the temperature gradients are managed appropriately to maximize the efficiency of the system.

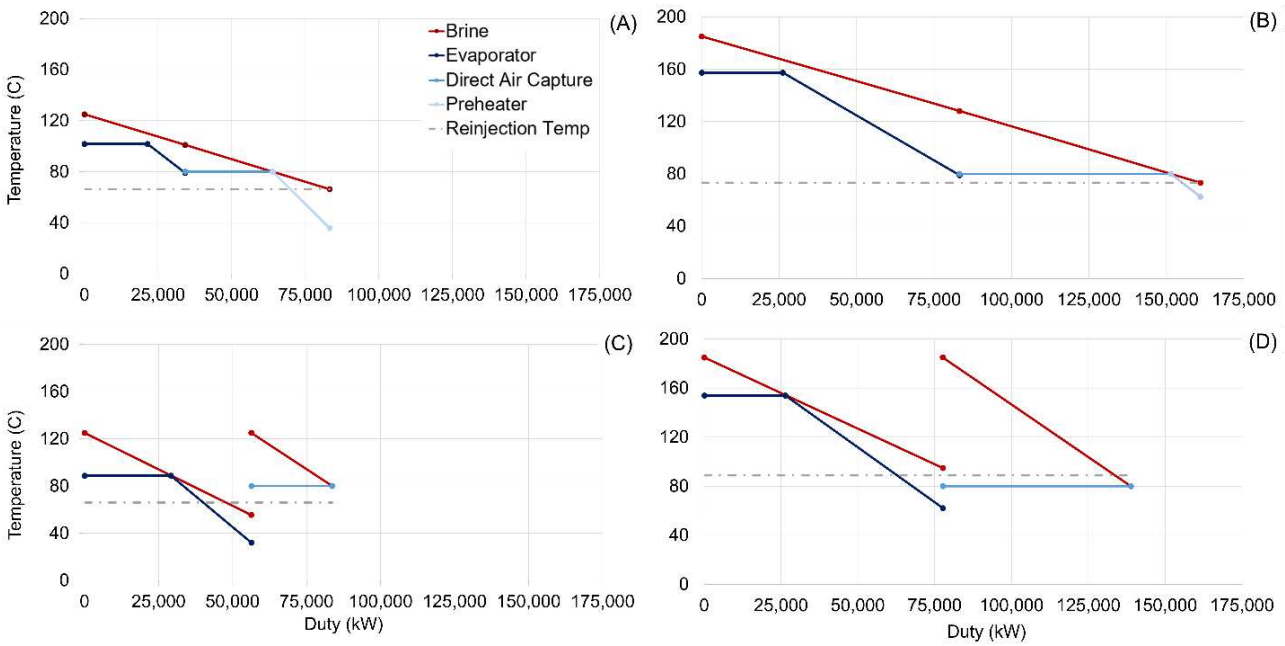

Figure 4-1: Temperature (°C) vs. Duty (kW) curves for representative geothermal reservoir temperatures and DAC in series vs. parallel configurations. **(A)** 125°C geothermal reservoir in series. **(B)** 185°C geothermal reservoir in series. **(C)** 125°C geothermal reservoir in parallel. **(D)** 185°C geothermal reservoir in parallel.

Figure 4-1C's brine temperature drops rapidly through the evaporator due to reduced mass flow in the parallel branch. This reduces the efficiency of both the ORC and overall DAC processes compared to Figure 4-1A, even though initial brine temperatures are the same. With more area between the curves in 4-1C, the cycle is unable to utilize the exergy of the brine in the most effective way. In Figure 4-1A, the brine goes directly to the evaporator allowing more efficient heat use before entering the DAC unit. Despite a low temperature brine entering the DAC, this configuration showed better heat utilization when compared to Figure 4-1C, seen by a more consistent temperature drop and less area between curves. In Figure 4-1D, despite the higher initial temperature, the brine still loses substantial heat, however the higher initial temperature provides higher relative exergy to the system, improving the ability to produce work in the turbine compared to Figure 4-1C and Figure 4-1A. Figure 4-1B maximizes the heat utilization, as the brine undergoes a controlled temperature drop through the evaporator and then to the DAC unit. This scenario

demonstrates the highest efficiency, with the brine fully utilizing its available exergy. Heat integrated series configurations (4-1A and 4-1B) are more efficient than split-stream parallel configurations (4-1C and 4-1D) as they allow for better utilization of the geothermal brine's relative exergy throughout the system. Higher reservoir temperatures in Figure 4-1B and Figure 4-1D naturally offer more available exergy in the brine to use for DAC, however the heat integrated configuration, Figure 4-1B, demonstrates the most efficient use of this energy, maximizing the performance of the ORC and DAC units. Split stream configurations (4-1C and 4-1D) show limitations due to the significant temperature drop after the initial heat extraction, reducing the effectiveness of the ORC and DAC process.

4.2. DAC Energy Source: Thermodynamic Performance and Economic Direct Comparison

4.2.1. EIA Capital Cost Estimates

Associated capital and operating costs were taken from the EIA "Capital Costs and Performance Characteristic Estimates for Utility Scale Electric Power Generating Technologies" report from February 2020. All costs were scaled to 2023 dollars to account for inflation between 2020 and 2023. Systems were scaled to a 30-year lifetime to provide a direct comparison across technologies.

Table 4-3: Geothermal CAPEX and OPEX breakdown, 50 MW system [15].

Capital Cost Assumptions		**Units**
EPC Contracting Fee	15%	% of Direct and Indirect Costs
Project Contingency	8%	% of Project Costs
Owners' Services	12%	% of Project Costs

Land Requirements	200	acres
Project Timeline		
Development, Permitting, Engineering	24	months
Operating Life	40	years
Cost Components		
Civil Structural Components	8,463,000	$
Mechanical Components	60,057,000	$
Steam Turbine	18,750,000	$
Projection/Injection System	21,644,000	$
Balance of Plant	19,663,000	$
Electrical Components	9,777,000	$
BOP and Miscellaneous	5,475,000	$
Substation and Switchyard	4,302,000	$
EPC Total	101,355,000	$
Project Indirect	9,838,000	$
EPC Total Before Fee	88,135,000	$
EPC Fee	13,220,000	$
Owners Cost Subtotal	15,363,000	$
Project Contingency	9,337,000	$
Total Capital Cost	126,055,000	$
Operating Cost Assumptions		**Units**
Labor	1,470,000	$/year
Steam Turbine Maintenance	3,750,000	$/year
Materials and Contract Servies	661,800	$/year
Admin and General	545,400	$/year
Land	2,000,000	$/year
Total Operating and Maintenance Costs	6,427,000	$/year

Table 4-4 outlines the EIA CAPEX and OPEX costs for solar PV and battery storage. Costs have also been scaled depending on energy demand for each case.

Table 4-4: Solar PV with battery energy storage EIA cost estimate breakdown, 150 MW with 200 MWh of lithium-ion battery storage [15].

Capital Cost Assumptions		**Units**
EPC Contracting Fee	5%	% of Direct and Indirect Costs
Project Contingency	5%	% of Project Costs
Owners' Services	4%	% of Project Costs
Land requirements	401	acres
Project Timeline		

Development, Permitting, Engineering	12	months
Operating Life	30	years
Cost Components		
Civil Structural Components	17,596,000	$
Mechanical Components	36,391,000	$
Racking, Tracking, Module Install		$
Electrical Components	105,350,000	$
Batteries	40,037,000	$
Inverters	14,459,000	$
BOP and Miscellaneous	28,453,000	$
Transformer, Substation, MV Station	18,647,000	$
Backup Power, Control and DAQ	3,755,000	$
EPC Total	171,716,000	$
Project Indirect	4,202,000	$
EPC Total Before Fee	163,539,000	$
EPC Fee	8,177,000	$
Owners Cost Subtotal	79,019,000	$
Project Contingency	12,537,000	$
Total Capital Cost	263,272,000	$
Operating Cost Assumptions		**Units**
Preventative Maintenance	1,545,000	$/year
Module Cleaning	613,000	$/year
Unscheduled Maintenance	115,000	$/year
Inverter Maintenance	455,000	$/year
Battery Maintenance	1,963,000	$/year
Land	4,825,000	$/year
Total Operating and Maintenance Costs	4,825,000	$/year

CAPEX and OPEX costs are shown in Table 4-5, outlining the various costs for implementing solar and batteries for the electricity required for DAC in the Geothermal+Firm Renewables case. Batteries are assumed to be replaced every 10 years and included in the cost analysis.

Table 4-5. Cost breakdown for the electricity infrastructure of the Geothermal+Firm Renewables case.

Reservoir Temperature (°C)	**DAC Regeneration**	**CAPEX Solar+Battery ($ M)**	**OPEX Solar+Battery ($ M/year)**	**Total CO_2 Removed (t-CO_2/year)**

	Temperature (°C)			
125	80	72.819	4.799	187,782
	100	49.912	3.289	128,815
	120	17.777	1.171	45,456
145	80	100.32	6.611	263,301
	100	81.320	5.359	213,640
	120	49.845	3.285	129,767
165	80	124.25	8.188	333,091
	100	104.45	6.883	281,331
	120	82.997	5.469	213,839
185	80	166.05	10.94	441,296
	100	144.76	9.539	388,585
	120	123.81	8.158	330,423
205	80	201.67	13.29	549,745
	100	180.84	11.92	492,288
	120	156.10	10.29	425,290

4.2.2. Integration of EIA and ASPEN Plus Cost Estimates

Component level costs for the ORC were used from ASPEN Plus. All other CAPEX costs for the geothermal system were incorporated from the EIA report. Table 4-6 shows the integration of ASPEN Plus economic data from the models and the EIA data for the geothermal power plant CAPEX and OPEX. The geothermal power plant cost for supplying thermal energy is shown as "EIA Geothermal Heating Only CAPEX" and standard across reservoir temperatures as it includes drilling costs, well costs, maintenance costs, labor costs, etc. CAPEX and OPEX costs included in the geothermal heat only scenarios do not include specific cost components related to ORCs and electricity generation from the ORC. The "EIA CAPEX Geothermal+ORC" includes other related ORC costs for the geothermal power plant including components the power plant needs for electricity generation. The "ASPEN ORC CAPEX" values are the component costs for the ORC at the various reservoir temperatures. These components are sized according to their performance and costed in ASPEN Plus. Integrating these two for the Geothermal+ORC case is shown in the "Total CAPEX (EIA+ASPEN)" column. The ASPEN Plus Process Economic Analyzer outputs

an operating cost for the system components (performance-based) and those values are denoted in the "ASPEN OPEX" column. Finally, the EIA report provides OPEX values for geothermal power plants for well maintenance, contract services, etc., and the total OPEX dependent on each case is shown in the "Total OPEX (EIA+ASPEN)" column. Land lease costs are not included here but are included in each respective DCF economic model for the LCOE for DAC value.

Table 4-6. Integration of ASPEN Plus and EIA geothermal CAPEX and OPEX costs.

Reservoir Temperature (°C)	Regeneration Temperature (°C)	EIA Geothermal Heating Only CAPEX ($ M)	EIA CAPEX Geothermal + ORC ($ M)	ASPEN ORC CAPEX ($ M)	Total CAPEX (EIA + ASPEN) ($ M)	OPEX ASPEN ($ M/year)	Total OPEX (EIA + ASPEN) ($ M/year)
125	80	413.95	428.19	13.054	441.24	2.1422	10.174
	100	413.95	428.19	7.9450	436.14	1.9301	9.9617
	120	413.95	428.19	4.7337	432.92	1.9630	9.9946
145	80	413.95	428.19	15.733	443.92	3.6569	11.689
	100	413.95	428.19	12.274	440.46	3.0741	11.106
	120	413.95	428.19	7.3882	435.58	1.9295	9.9611
165	80	413.95	428.19	13.450	441.64	3.8469	11.878
	100	413.95	428.19	11.698	439.89	3.4122	11.444
	120	413.95	428.19	8.3642	436.55	2.5156	10.547
185	80	413.95	428.19	19.576	447.77	5.0738	13.105
	100	413.95	428.19	16.211	444.40	4.5209	12.553
	120	413.95	428.19	13.596	441.79	4.0861	12.118
205	80	413.95	428.19	20.380	448.57	5.5425	13.574
	100	413.95	428.19	17.460	445.65	5.1041	13.136
	120	413.95	428.19	15.131	443.32	4.5538	12.585

Capital cost estimates for the geothermal power plant may have some variations due to significant upfront costs of drilling, infrastructure, and installation costs. These costs are generally highly variable and site-specific. A sensitivity analysis could help identify how variation in cost drivers impact overall CAPEX. Future work of implementing these sensitivity values into the TEA would benefit economic viability assessments and investment decisions to understand how these cost drivers influence payback periods and net present values.

4.2.3. Grid Electricity Cost Breakdown

Grid electricity costs were determined using NVEnergy's pricing schedule outlined in Table 4-7. Although NVEnergy is a specific electricity provider, geothermal-DAC systems are particularly well-suited for deployment in Nevada due to its extensive geothermal resources highlighted in Figure 1-1, therefore this pricing schedule was used for the analysis. The total electricity costs were calculated by incorporating both required standard energy demand charges in addition to demand charges to reflect operational costs under full system operation.

Table 4-7: NVEnergy Electricity Rate Schedule [16]**.**

Electricity Charge	**Value**	**Unit**
Basic Service Charge	536.60	$/month
Facilities Charge	6.50	$/kW
Demand Charge		
Winter All Hours	1.46	$/kW
Summer On-Peak (June 1- Sept. 30) (3pm-9pm)	13.62	$/kW
Summer Off-Peak (June 1 – Sept. 30) (All other hours)	4.14	$/kW
Electric Consumption		
Summer On Peak (June 1- Sept. 30) (3pm-9pm)	0.168	$/kW
Summer Off Peak (June 1 – Sept. 30) (All other hours)	0.085	$/kW
Winter All Hours	0.072	$/kW

CAISO wholesale electricity costs had an average of $0.0516/kWh [74] in 2023 and the normalized cost for NVEnergy using Table 4-7 pricing schedule was calculated to be $0.195/kWh. Although this electricity cost is 3.8 times wholesale costs, using a utility provider electricity schedule provides a better representation of utilizing grid electricity for an intensive process like DAC.

Table 4-8 provides the LCOE values for DAC for the 4 scenarios analyzed throughout the study and represents the values plotted in Figure 4-2. Costs are shown with varying reservoir temperatures and varying regeneration temperatures for the geothermal cases.

Table 4-8: Levelized cost of energy for DAC ($/t-$CO_2$ removed) values for various renewable energy scenarios.

	Geothermal+ORC			**Geothermal+Firm Renewables**			**Solar+Battery**			**Geothermal+Grid Electricity**		
	80°C	**100°C**	**120°C**	**80°C**	**100°C**	**120°C**	**80°C**	**100°C**	**120°C**	**80°C**	**100°C**	**120°C**
125°C	176.43	253.29	719.67	154.73	207.92	519.05	175.90	175.90	175.90	230.06	293.22	664.51
145°C	132.21	158.74	249.98	120.72	139.95	206.34	175.90	175.90	175.90	188.33	211.06	290.60
165°C	103.69	120.28	152.24	102.55	114.43	140.60	175.90	175.90	175.90	165.31	179.03	213.39
185°C	82.70	91.26	105.71	86.81	93.14	103.25	175.90	175.90	175.90	147.29	154.11	166.45
205°C	66.57	73.05	82.71	76.11	80.79	87.75	175.90	175.90	175.90	133.00	138.61	146.76

Figure 4-2 illustrates the LCOE for DAC across different geothermal brine temperatures and regeneration temperatures for the various renewable energy scenarios.

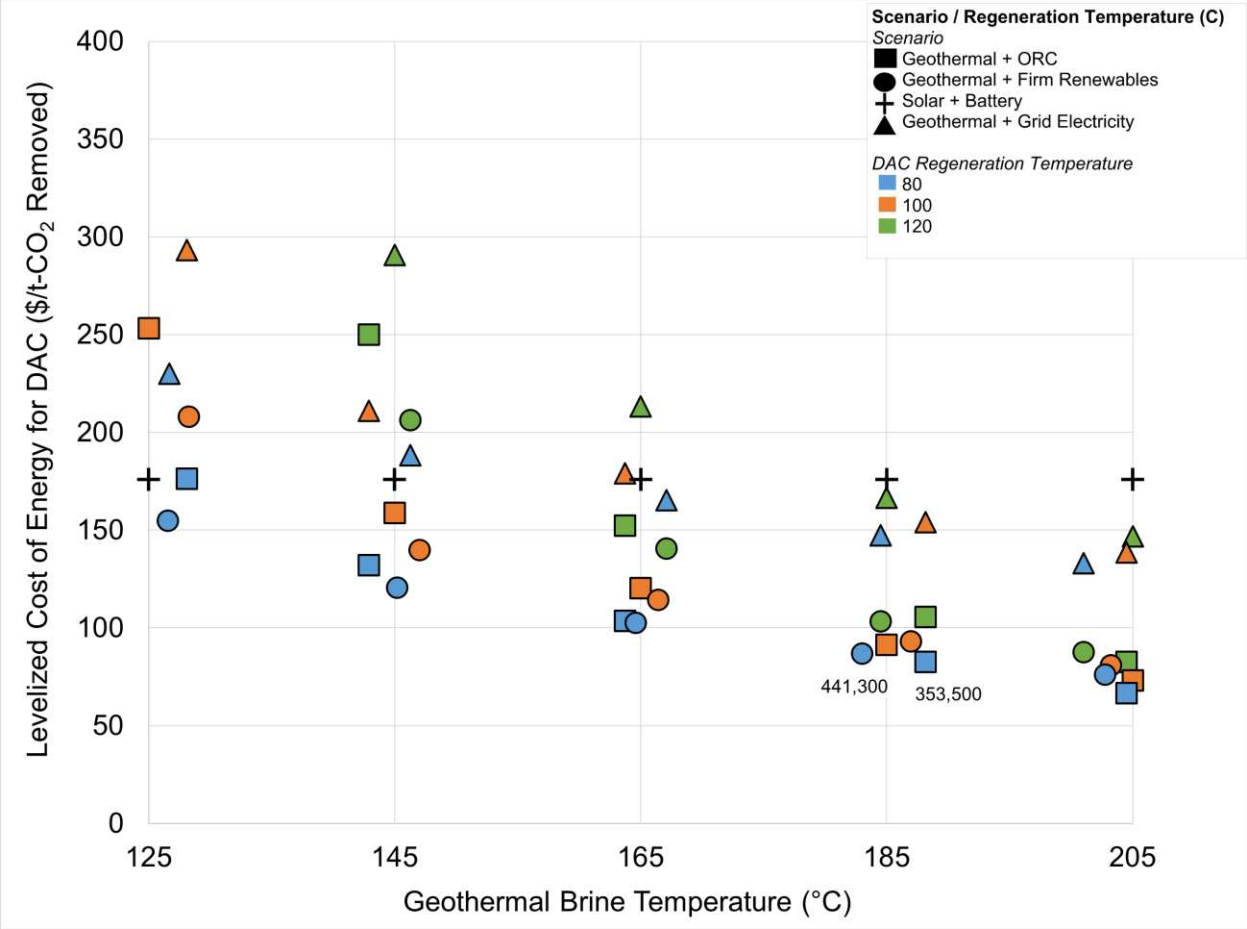

Figure 4-2: Levelized cost of energy for direct air capture across various energy input scenarios with varied reservoir temperature and varied DAC regeneration temperature. Values shown for t-CO_2 removed annually for Geothermal+ORC case (blue circle) and Geothermal+Firm Renewables (blue square) at 80°C regeneration temperature.

Understanding geothermal limitations compared to other renewable energy sources directly informs decision-making when integrating DAC. At lower reservoir temperatures and higher regeneration temperatures, Geothermal+Firm Renewables (in the form of solar and batteries) outperforms Geothermal+ORC. Geothermal+ORC at 125°C and a 100°C regeneration temperature has a levelized cost of \$253.29/t-CO_2 removed, while Geothermal+Firm Renewables is \$207.92/t-CO_2 removed. Additionally, at a 125°C reservoir and 120°C regeneration temperature, Geothermal+Firm Renewables performs better than Geothermal+ORC by almost \$200/t-CO_2

removed. However, at a 185°C reservoir temperature and 80°C regeneration temperature, Geothermal+ORC is \$82.70/t-CO_2 removed while Geothermal+Firm Renewables is \$86.81/t-CO_2 removed. Geothermal+ORC outperforms Geothermal+Firm Renewables at all three regeneration temperatures at reservoirs above 185°C. It is expected that Geothermal+ORC would continue to be most cost-effective as reservoir temperatures increase past the highest tested value of 205°C. The ORC becomes more cost effective as reservoir temperatures increase and regenerations temperatures decrease when evaluated against Geothermal+Firm Renewables. In lower reservoir temperatures, Geothermal+Firm Renewables performs better than all other scenarios. At 165°C reservoir and 80°C regeneration, Geothermal+Firm Renewables is \$102.55/t-CO_2 removed while Geothermal+ORC is \$103.69/t-CO_2 removed. Utilizing geothermal heat for the heating requirements of DAC and sourcing electricity elsewhere proves to be beneficial at lower and middle grade reservoir temperatures. The CO_2 removal benefit outweighs the additional CAPEX investment as more CO_2 is removed from the atmosphere when supplying all geothermal heat for the heating requirements of DAC.

In scenarios with low-temperature geothermal reservoirs, Solar+Battery is more cost-effective than geothermal-based solutions, specifically at higher DAC regeneration temperatures, due to the high capital investment required for a geothermal plant, yet with limited exergy available. At a 125°C reservoir and 120°C regeneration temperature, Solar+Battery for both heat and electricity is most economical at \$175.90/t-CO_2 removed, compared to \$719.67/t-CO_2 removed for the Geothermal+ORC system and \$519.05/t-CO_2 removed for Geothermal+Firm Renewables. The reduced efficiency of ORC systems at lower geothermal brine temperatures is attributed to the smaller temperature gradient between heat source and ambient, resulting in lower thermodynamic efficiency, and consequently higher energy costs. Given the high capital costs of turbines, optimal

efficiency is critical to justify the investment cost. In contrast, solar and battery systems provide a clean, consistent, and reliable energy source for the DAC electricity requirements, bypassing any efficiency losses associated with low-temperature geothermal systems. In this context, the lower efficiency of ORC electricity generation at low temperatures makes Solar+Battery more cost-effective, leveraging the renewable energy more effectively. The additional CAPEX of the solar and batteries is offset by the inefficiencies inherent in low temperature ORC systems, resulting in a more economical solution for DAC electricity demand.

At higher reservoir temperatures, Geothermal+ORC is optimal. The higher reservoir temperature significantly improves the ORC system efficiency. A larger temperature difference between the brine and ambient allows for more effective heat conversion to work, enhancing thermodynamic efficiency. Generating more power reduces the LCOE, making Geothermal+ORC configurations more optimal at these higher brine temperatures. Increased power and efficiency mean relative costs of the ORC system decrease, making it a more cost-effective option when compared to the additional capital investment of solar and batteries, and more heat is available for capturing CO_2. Capturing more CO_2 directly enhances the LCOE because more output is generated at the same investment cost.

Lowering regeneration temperatures is crucial for enhancing efficiency in DAC systems. Reducing the regeneration temperature allows for more captured CO_2 from the sorbent, lowering both the energy demand and the overall system cost. Additionally, this approach enhances compatibility with low-grade heat sources, allowing for broader utilization of the available thermal heat.

The Geothermal+Grid Electricity configuration is not cost-effective in any scenario primarily due to emissions associated with grid electricity and elevated electricity pricing on the open

market. Figure 4-3 breaks down the United States grid intensity in terms of CO_2 emissions per kWh (gCO_2/kWh) across different electricity markets [75]. The regions with higher grid intensity (towards the left of the graph) emit more CO_2, indicating a heavier reliance on fossil fuels with higher CO_2 emissions. Regions on the right have a lower grid intensity and likely have a greater proportion of renewable energy sources in the electricity mix. The grid emissions factor used in this research was the 2023 average U.S. grid emissions of 460 gCO_2/kWh.

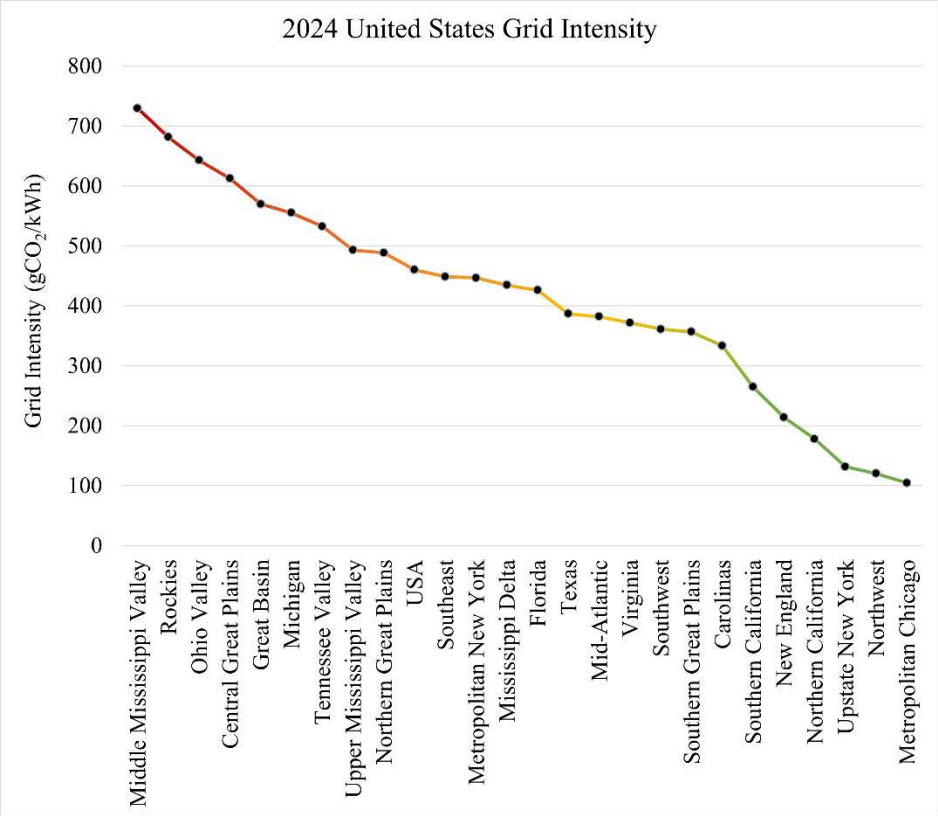

Figure 4-3: United States electricity market associated grid emissions in 2024.

Reliance on grid electricity, often from fossil fuels, results in CO_2 emissions, which contradicts the primary objective of DAC [76]. Emissions are calculated using Equation 8 to quantify the relationship between production rate and the grid *EF*.

$$M_{t,Geo+Grid} = M_t - (E_{DAC} \times EF_{Grid}) \quad (8)$$

The grid emissions for each Geothermal+Grid Electricity case is shown in Table 4-9.

Table 4-9: Total CO_2 removed for Geothermal+Grid Electricity case.

Reservoir Temperature (°C)	**DAC Regeneration Temperature (°C)**	**Total DAC CO_2 Removed (M_t) (t-CO_2/year)**	**Associated Grid Emissions (t-CO_2/year)**	**Total CO_2 Removed ($M_{t,Geo+Grid}$) (t-CO_2/year)**
125	80	187,782	25,503	162,279
	100	128,816	17,480	111,335
	120	45,456	6,226	39,230
145	80	263,302	35,136	228,165
	100	213,640	28,481	185,159
	120	129,767	17,457	112,310
165	80	333,091	43,516	289,575
	100	281,331	36,580	244,751
	120	213,840	29,068	184,771
185	80	441,297	58,157	383,140
	100	388,586	50,698	337,887
	120	330,423	43,361	287,062
205	80	549,746	70,633	479,113
	100	492,288	63,334	428,953
	120	425,290	54,671	370,618

For this case, variable grid pricing coupled with high demand charges, reduces its suitability for DAC applications. This highlights the importance of aligning energy sources with their most efficient and cost-effective uses to optimize economic and environmental outcomes.

4.3. Discounted Cash Flow: Solar+Battery Renewable Energy Baseline

An example DCF is shown in Table 4-10. The representative case outlined is for Solar+Battery, however, all LCOE for DAC estimates use a similar cash flow with respective input and output costs. DCFs for the other cases are shown in Appendix B. The capacity factor for the Solar+Battery case is 16% [77].

Table 4-10: DCF for the Solar+Battery case projected out 30 years.

	-2	**-1**	**0**	**1**	**2**	**3**	**4**

Equipment and Facilities Cost ($ M)	153.49	153.49	153.49				
Loan Interest Payment ($ M)	18.418	36.837	55.255	55.813	55.049	54.225	53.334
Loan Principle ($ M)	230.23	460.46	690.69	688.12	677.81	666.68	654.66
Annual Cost ($ M)	17.273	17.273	17.273	17.273	17.273	17.273	17.273
Discount Factor	1.21	1.1	1	0.90909	0.82645	0.75131	0.68301
Annual Present Value ($ M)				194.30	202.05	151.65	130.46
Total Capital Investment + Interest ($ M)	208.00	209.35	208.74				
Operating Costs Net Present Value ($ M)				15.703	14.275	12.977	11.797
Capital Costs Net Present Value ($ M)	185.72	168.83	153.49				

	5	**6**	**7**	**8**	**9**	**10**	**11**
Loan Interest Payment ($ M)	52.373	51.334	50.212	49.001	47.692	46.279	44.753
Loan Principle ($ M)	641.68	627.65	612.51	596.15	578.49	559.41	538.81
Annual Cost ($ M)	17.273	17.273	17.273	17.273	17.273	17.273	17.273
Discount Factor	0.62092	0.56447	0.51315	0.46650	0.42409	0.38554	0.35049
Annual Present Value ($ M)	118.418	97.179	78.829	71.465	64.774	58.695	53.171
Operating Costs Net Present Value ($ M)	10.725	9.7502	8.8638	8.0580	7.3254	6.6595	6.0541

	12	**13**	**14**	**15**	**16**	**17**	**18**
Loan Interest Payment ($ M)	43.105	41.325	39.402	37.326	35.084	32.662	30.046
Loan Principle ($ M)	516.56	492.53	466.57	438.54	408.27	375.58	340.27
Annual Cost ($ M)	17.273	17.273	17.273	17.273	17.273	17.273	17.273
Discount Factor	0.31863	0.28966	0.2633	0.23939	0.21762	0.19784	0.17985
Annual Present Value ($ M)	48.154	43.596	39.455	35.694	32.279	29.177	26.360
Operating Costs Net Present Value ($ M)	5.5037	5.0034	4.5485	4.1350	3.7591	3.4174	3.1067

	19	**20**	**21**	**22**	**23**	**24**	**25**
Loan Interest Payment ($ M)	27.221	24.171	20.876	17.317	13.474	9.3238	4.8412
Loan Principle ($ M)	302.13	260.95	216.47	168.43	116.55	60.515	(0)
Annual Cost ($ M)	17.273	17.273	17.273	17.273	17.273	17.273	17.273
Discount Factor	0.16350	0.14864	0.13513	0.12284	0.11167	0.10152	0.09229
Annual Present Value ($ M)	23.802	21.479	19.371	17.457	15.719	14.143	12.712
Operating Costs Net Present Value ($ M)	2.8243	2.5675	2.3341	2.1219	1.9290	1.7537	1.5942

	26	**27**	**28**	**29**
Loan Interest Payment ($ M)	(0)	(0)	(0)	(0)
Loan Principle ($ M)	(0)	(0)	(0)	(0)
Annual Cost ($ M)	17.273	17.273	17.273	17.273
Discount Factor	0.08390	0.07627	0.06934	0.06303
Annual Present Value ($ M)	16.898	15.362	13.966	12.696
Operating Costs Net Present Value ($ M)	1.4493	1.3175	1.1978	1.0889

CAPEX components are broken down in Table 4-11 to understand expenses for this specific Solar+Battery case. All represented cases have CAPEX and OPEX breakdowns respective to their system components.

Table 4-11. Solar+Battery CAPEX components breakdown.

Category	Specific Components
Electrical Infrastructure	Internal and control connections
	Onsite electrical equipment
	Power electronics
	Wiring and installation
	Inverters
	Switch gear
	Transformers
	Energy management system
	Monitors, controls, communications
Generation Equipment and Infrastructure	Plant construction
	Power plant equipment
	Foundation
	Hardware
	Module supply
	Racking
	Battery pack
	Battery container
	Battery and thermal management system
	Fire suppression system
	Battery racking
	Inverter housing
Installation & Indirect	Distributable labor and materials
	Engineering
	Start up and commissioning
Owner's Costs	Development costs
	Environmental studies and permitting
	Insurance costs
	Legal fees
	Preliminary feasibility and engineering studies
	Property taxes during construction
Site	Buildings for operation and maintenance
	Transformers
	Underground utilities

4.4. Levelized Cost Breakdown: Renewable Energy Cases

The levelized cost of the 4 renewable energy cases are broken down in Figure 4-4 by levelized cost of energy contribution to the overall LCOE for DAC. The represented case is 165°C reservoir temperature and 100°C regeneration temperature. Total CO_2 removed is also shown on

the secondary y-axis to understand the relationship between production rate and levelized cost for specific technologies.

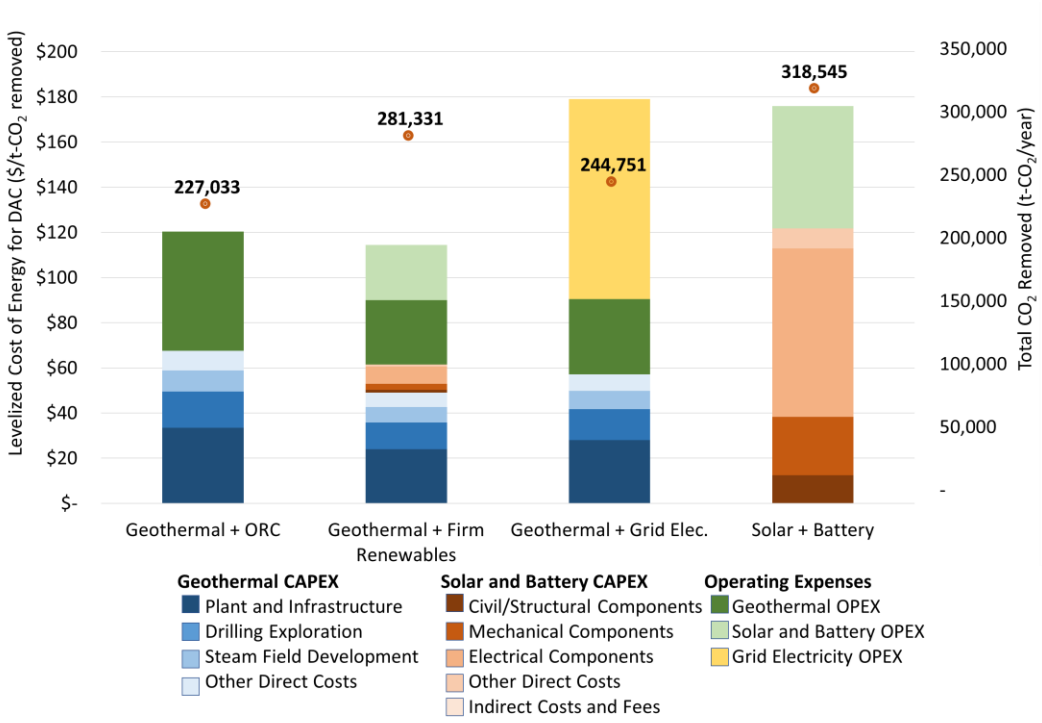

Figure 4-4: Levelized cost of energy for DAC proportional breakdown of CAPEX and OPEX for a 165°C reservoir and 100°C DAC regeneration of renewable energy scenarios for DAC with total CO_2 removed annually across each scenario.

Figure 4-4 analyzes the levelized cost per component for CAPEX and OPEX (lifetime cost) in each scenario. The Geothermal+ORC has a high CAPEX, with an LCOE contribution of $33.47 due to high plant and infrastructure expenses and drilling costs with an LCOE contribution of $16.04. However, once operational, the system benefits from low OPEX and stable performance. The ORC optimizes geothermal heat use especially at temperatures above 165°C, enhancing energy efficiency and lowering overall costs by removing more CO_2 from the atmosphere with the available infrastructure. The Geothermal+Firm Renewables case leverages geothermal heat with the reliability of solar and batteries for the electricity needed. The poorer efficiency of the ORC at

lower temperatures of 125°C and 145°C highlighted in Figure 4-2 justifies additional CAPEX for the solar and batteries for the Geothermal+Firm Renewables case. Although additional solar and battery CAPEX increases initial upfront investment, the ability to remove more CO_2 under the same geothermal reservoir conditions outweighs using an ORC for both DAC heat and electricity requirements. This presents an LCOE contribution for solar and battery CAPEX of $12.37 and an OPEX LCOE contribution of $24.46, with a majority of this OPEX contribution being from every 10-year battery replacement.

Although the Solar+Battery case removes the most CO_2 annually, the initial upfront investment of the solar and batteries needed for this large-scale system makes the Geothermal+ORC and Geothermal+Firm Renewables case perform better under these conditions. Finally, the high operating expenses of $88.60 for the Geothermal+Grid electricity case including the variability with grid reliability and emissions associated with the grid electricity makes this case unfavorable when compared to the other geothermal coupled cases. Accounting for grid emissions lowers the total CO_2 removed to 244,751 tons annually for this case, directly impacting the driver for LCOE. There is a key balance between high initial capital investment with long-term operational savings, especially when being projected out 30 years. The efficiency improvements using ORCs at high temperatures combined with their lower operating expenses outweighs the benefits seen in other scenarios. This figure highlights the investment considerations for deploying geothermal energy for DAC. As shown, geothermal capital cost remains relatively consistent across all regardless of the reservoir temperature, because essential infrastructure – such as wells, drilling, and structural components are required in all cases. Therefore, utilizing a geothermal resource with higher exergy improves the systems performance and benefits the overall LCOE for DAC due to the ability to remove more CO_2 from the atmosphere annually. Understanding geothermal power plant CAPEX

considerations is vital in guiding geothermal-DAC energy source decisions because of this high investment cost, independent of the resource temperature.

4.5. Levelized Cost Breakdown: Geothermal Cases

The breakdown for all the components of Figure 4-5 is shown in Table 4-12. The geothermal CAPEX is broken up into respective categories and OPEX values are included as one data value for this analysis.

Table 4-12: Levelized cost of energy for DAC contribution breakdown.

Levelized Cost Contribution Breakdown	**145°C**		**185°C**	
	80°C	**120°C**	**80°C**	**120°C**
Plant and Infrastructure	$33.91	$68.53	$19.99	$26.50
Drilling Exploration	$16.96	$33.92	$10.13	$13.32
Steam Field Development	$9.89	$19.79	$5.91	$7.77
Turbine Cost	$0.72	$0.73	$0.70	$0.70
Other Direct Costs	$9.19	$18.37	$5.49	$7.22
Geothermal OPEX	$61.55	$108.65	$40.47	$50.20

Figure 4-5 breaks down the LCOE for DAC for the Geothermal+ORC case across two reservoir temperatures, 145°C and 185°C, and 2 different DAC regeneration temperatures, 80°C and 120°C. Additionally, the total CO_2 removed per year is shown on the secondary y-axis to understand the production rate of these different cases and how it affects the contributions to the LCOE for DAC.

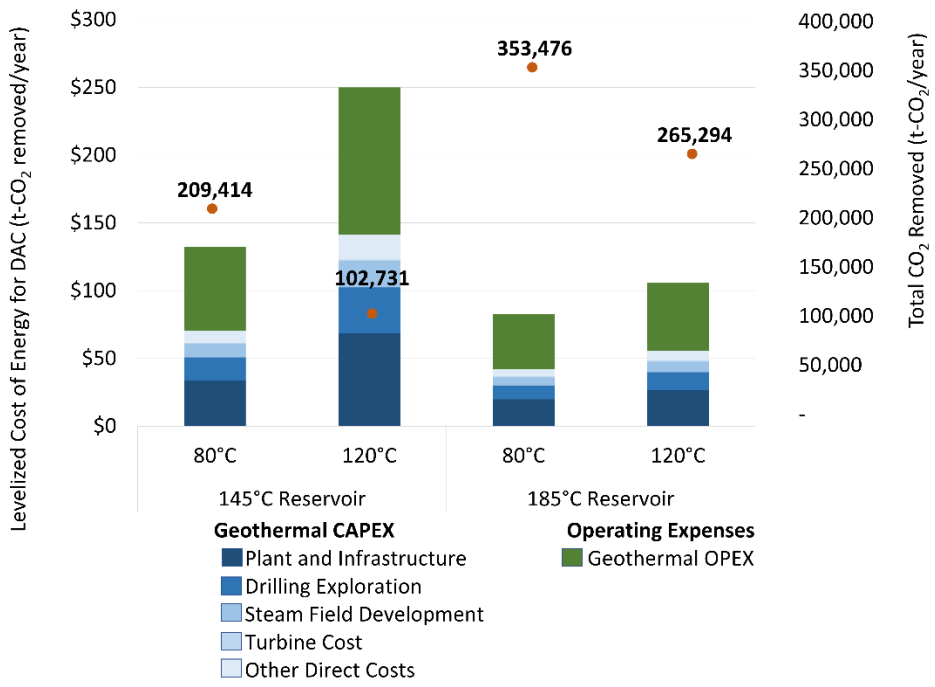

Figure 4-5: Levelized cost of DAC proportional breakdown of Geothermal+ORC for 145°C and 185°C reservoir and 80°C and 120°C DAC regeneration temperature with total CO_2 removed annually.

The ability to remove higher amounts of CO_2 annually drastically improves the levelized cost. The total CO_2 removed at the same 145°C reservoir and 80°C regeneration is 209,414 tonnes/year compared to 353,476 tonnes/year when regeneration is 120°C. Having a high reservoir temperature and a lower DAC regeneration temperature is favorable due to its ability to remove greater amounts of CO_2 from the atmosphere for the same well size. Even though the CAPEX and OPEX of geothermal infrastructure such as the turbine and its maintenance are greater at higher reservoir temperatures, the CO_2 removal benefits offset the additional costs shown in Figure 5B. While the geothermal capital cost is about the same, the CAPEX LCOE contribution is close to double because the amount of CO_2 removed is nearly half. Higher temperature systems also offer greater potential scalability with CO_2 removal which makes them more suitable for large scale implementation [37], imperative for reaching IPCC climate goals. Making investment decisions is

crucial for energy sources when coupled with DAC, and despite higher initial investments, scaling these plants with higher geothermal temperature reservoirs is advantageous with regards to environmental and economic success.

CHAPTER 5. Conclusion

5.1. Summary of Findings

Low-cost and high CO_2 removal technology configurations are necessary to successfully deploy DAC while meeting IPCC climate goals. High geothermal reservoir temperatures and low regeneration temperatures benefit DAC technology, as shown in Figure 4-2. Determining which configuration is optimal depends on several factors including the availability of resources, the type of sorbent being used for regeneration to achieve lower regeneration temperatures, CAPEX/OPEX tradeoffs, and investment in separate renewable energy sources for electricity generation. This research validates that geothermal heat is highly effective for DAC heating requirements. Additionally, the economic analysis indicates that firm renewables are more cost-efficient for meeting DAC electricity needs at lower and moderate reservoir temperatures, while ORCs are effective at higher reservoir temperatures.

5.2. Limitations and Recommendations for Future Work

Limitations in this work include the working fluids evaluated for the ORC. More robust optimization is necessary to understand which working fluids perform better at higher and lower reservoir temperatures. Additionally, manual optimization is suitable for this analysis, but future work would benefit from a computational optimization model of the geothermal-DAC coupled system. Finally, implementing a sensitivity analysis of the CAPEX costs for geothermal and the other renewable energy sources would be beneficial to account for variation in drilling, infrastructure, and installation costs, to account for regional cost differences as well.

The integration of DAC with renewable energy systems has substantial potential for achieving decarbonization objectives. Potential future work can incorporate heat pumps into the firm renewables case, which can upgrade low grade heat into a useable form for DAC applications. In addition, a comprehensive understanding of the evolving electric grid and its emissions could

guide deployment of decarbonization technologies. An analysis on electricity cost would be beneficial to understand demand periods and running alternative technologies during these high cost periods. The electricity cost for the representative case makes up close to half the levelized cost contribution so finding alternatives to making this electricity cost cheaper could potentially improve economics of this case. Additional research for geographic optimization, including pipeline availability, subsurface storage formations for CO_2 storage and solar resource availability could improve understanding of geographical constraints. DAC is attractive because it can be placed anywhere, though locational analysis could identify optimal locations to improve system performance and cost-effectiveness. The results from this analysis do not incorporate storage and transportation costs, although they can be close to \$15/ton CO_2. This research would benefit from a geological mapping with pipelines or subsurface formation sites that could quantify transport and storage costs depending on mileage. This would give insight into the full cycle of capturing CO_2 and a better estimation of costs including end of life cost for storing or transporting CO_2. Quantifying non-monetary benefits such as reduced land area could improve understanding of tradeoffs between different technologies. Additionally, a comparison between renewable energy technologies and non-renewable energies for use in carbon capture and storage is important to understand the future of implementing these technologies. Solid sorbent DAC has great potential to be implemented with geothermal energy alongside other renewables however, using natural gas combined cycle (NGCC) with carbon capture and storage can be an effective energy source to fulfil demands for DAC as well. Costs for NGCC with DAC are about \$116/MWh [31]. A further evaluation and looking at other energy sources besides renewables are vital when directly comparing technologies in the techno-economic analysis. Finally, incorporating community engagement and listening sessions would ensure social responsibility and sustainable

implementation to communities affected by such infrastructure. These recommended enhancements to the work could benefit the transformative potential of integrating geothermal with DAC and other renewable energy resources, providing a pivotal framework in global decarbonization efforts.

REFERENCES

[1] R. Hanna, A. Abdulla, Y. Xu, and D. G. Victor, "Emergency deployment of direct air capture as a response to the climate crisis," *Nat Commun*, vol. 12, no. 1, Dec. 2021, doi: 10.1038/s41467-020-20437-0.

[2] R. Chauvy and L. Dubois, “Life cycle and techno-economic assessments of direct air capture processes: An integrated review,” Jun. 25, 2022, *John Wiley and Sons Ltd*. doi: 10.1002/er.7884.

[3] J. Rogelj, “Mitigation Pathways Compatible with 1.5°C in the Context of Sustainable Development,” in *Global Warming of 1.5°C*, Cambridge University Press, 2022, pp. 93–174. doi: 10.1017/9781009157940.004.

[4] C. Beuttler, L. Charles, and J. Wurzbacher, “The Role of Direct Air Capture in Mitigation of Anthropogenic Greenhouse Gas Emissions,” *Frontiers in Climate*, vol. 1, Nov. 2019, doi: 10.3389/fclim.2019.00010.

[5] M. Zeeshan, M. K. Kidder, E. Pentzer, R. B. Getman, and B. Gurkan, “Direct air capture of CO2: from insights into the current and emerging approaches to future opportunities,” *Frontiers in Sustainability*, vol. 4, 2023, doi: 10.3389/frsus.2023.1167713.

[6] J. Fuhrman *et al.*, “Diverse carbon dioxide removal approaches could reduce impacts on the energy–water–land system,” *Nat Clim Chang*, vol. 13, no. 4, pp. 341–350, Apr. 2023, doi: 10.1038/s41558-023-01604-9.

[7] B. Sigfússon, M. Þ. Arnarson, S. Ó. Snæbjörnsdóttir, M. R. Karlsdóttir, E. S. Aradóttir, and I. Gunnarsson, “Reducing emissions of carbon dioxide and hydrogen sulphide at Hellisheidi power plant in 2014-2017 and the role of CarbFix in achieving the 2040 Iceland climate goals,” *Energy Procedia*, vol. 146, pp. 135–145, Jul. 2018, doi: 10.1016/j.egypro.2018.07.018.

[8] J. F. Wiegner, A. Grimm, L. Weimann, and M. Gazzani, “Optimal Design and Operation of Solid Sorbent Direct Air Capture Processes at Varying Ambient Conditions,” *Ind Eng Chem Res*, 2022, doi: 10.1021/acs.iecr.2c00681.

[9] M. Fasihi, O. Efimova, and C. Breyer, “Techno-economic assessment of CO 2 direct air capture plants,” *J Clean Prod*, vol. 224, pp. 957–980, Jul. 2019, doi: 10.1016/j.jclepro.2019.03.086.

[10] C. Breyer, M. Fasihi, and A. Aghahosseini, “Carbon dioxide direct air capture for effective climate change mitigation based on renewable electricity: a new type of energy system sector coupling,” *Mitig Adapt Strateg Glob Chang*, vol. 25, no. 1, pp. 43–65, Jan. 2020, doi: 10.1007/s11027-019-9847-y.

[11] S. J. Zarrouk and H. Moon, “Efficiency of geothermal power plants: A worldwide review,” *Geothermics*, vol. 51, pp. 142–153, Jul. 2014, doi: 10.1016/j.geothermics.2013.11.001.

[12] K. F. Beckers, A. Kolker, H. Pauling, J. D. McTigue, and D. Kesseli, “Evaluating the feasibility of geothermal deep direct-use in the United States,” *Energy Convers Manag*, vol. 243, Sep. 2021, doi: 10.1016/j.enconman.2021.114335.

[13] C. F. Williams, M. J. Reed, R. H. Mariner, J. DeAngelo, and S. Peter Galanis, “Assessment of Moderate-and High-Temperature Geothermal Resources of the United States”.

[14] R. Zehner, M. Coolbaugh, and Shevenellm Lisa, “Preliminary geothermal potential and exploration activity in Nevada,” *NBMG Publications*, 2009.

[15] U. Energy Information Administration, “Capital Cost and Performance Characteristic Estimates for Utility Scale Electric Power Generating Technologies,” 2020. [Online]. Available: www.eia.gov

[16] NVEnergy, “Sierra Pacific Power Company d/b/a NV Energy Standard Electric Rate Schedules for General/Commercial Customers,” 2023.

[17] E. O’shaughnessy, J. Heeter, and J. Sauer, “Status and Trends in the U.S. Voluntary Green Power Market (2017 Data),” 2018. [Online]. Available: www.nrel.gov/publications.

[18] Nexamp, “Solar Renewable Energy Credits: SREC Programs & Prices.”

[19] LevelTen Energy, “North American Solar and Wind PPA Prices Increased 6.6% in Q1 of 2023, Marking Two Years of Rising Prices, According to LevelTen Energy.”

[20] Office of Fossil Energy and Carbon Management, “Carbon Dioxide Removal.”

[21] D. R. Morrow *et al.*, “Principles for Thinking about Carbon Dioxide Removal in Just Climate Policy,” *One Earth*, vol. 3, no. 2, pp. 150–153, Aug. 2020, doi: 10.1016/j.oneear.2020.07.015.

[22] United States Environmental Protection Agency, “Sources of Greenhouse Gas Emissions.”

[23] K. An, K. Li, C.-M. Yang, J. Brechtl, and K. Nawaz, “A comprehensive review on regeneration strategies for direct air capture,” *Journal of CO2 Utilization*, vol. 76, p. 102587, Oct. 2023, doi: 10.1016/j.jcou.2023.102587.

[24] D. W. Keith, G. Holmes, D. St. Angelo, and K. Heidel, “A Process for Capturing CO2 from the Atmosphere,” *Joule*, vol. 2, no. 8, pp. 1573–1594, Aug. 2018, doi: 10.1016/j.joule.2018.05.006.

[25] N. McQueen, K. V. Gomes, C. McCormick, K. Blumanthal, M. Pisciotta, and J. Wilcox, “A review of direct air capture (DAC): Scaling up commercial technologies and innovating for the future,” Jul. 01, 2021, *Institute of Physics*. doi: 10.1088/2516-1083/abf1ce.

[26] M. Broehm, J. Strefler, and N. Bauer, “Techno-Economic Review of Direct Air Capture Systems for Large Scale Mitigation of Atmospheric CO2 Techno-Economic Review of Direct Air Capture Systems for Large Scale Mitigation of Atmospheric CO 2.” [Online]. Available: https://ssrn.com/abstract=2665702

[27] Y. Ishimoto, M. Sugiyama, E. Kato, R. Moriyama, K. Tsuzuki, and A. Kurosawa, “Putting Costs of Direct Air Capture in Context | FCEA Working Paper No. 2,” 2017.

[28] T. Kuru, K. Khaleghi, and S. Livescu, “Solid sorbent direct air capture using geothermal energy resources (S-DAC-GT) – Region specific analysis,” *Geoenergy Science and Engineering*, vol. 224, May 2023, doi: 10.1016/j.geoen.2023.211645.

[29] N. McQueen *et al.*, “Cost Analysis of Direct Air Capture and Sequestration Coupled to Low-Carbon Thermal Energy in the United States,” *Environ Sci Technol*, vol. 54, no. 12, pp. 7542–7551, Jun. 2020, doi: 10.1021/acs.est.0c00476.

[30] S. Brandani, “CARBON DIOXIDE CAPTURE FROM AIR: A SIMPLE ANALYSIS.”

[31] K. Z. House, A. C. Baclig, M. Ranjan, E. A. Van Nierop, J. Wilcox, and H. J. Herzog, “Economic and energetic analysis of capturing CO 2 from ambient air,” 1998, doi: 10.1073/pnas.1012253108/-/DCSupplemental.

[32] A. Alabdulkarem, Y. Hwang, and R. Radermacher, “Multi-functional heat pumps integration in power plants for CO2 capture and sequestration,” *Appl Energy*, vol. 147, pp. 258–268, Jun. 2015, doi: 10.1016/j.apenergy.2015.03.003.

[33] A. J. Simon, N. B. Kaahaaina, S. J. Friedmann, and R. D. Aines, “Systems analysis and cost estimates for large scale capture of carbon dioxide from air,” in *Energy Procedia*, Elsevier Ltd, 2011, pp. 2893–2900. doi: 10.1016/j.egypro.2011.02.196.

[34] A. Ebrahimi, B. Ghorbani, and M. Taghavi, “Novel integrated structure consisting of CO2 capture cycle, heat pump unit, Kalina power, and ejector refrigeration systems for liquid CO2 storage using renewable energies,” *Energy Sci Eng*, vol. 10, no. 8, pp. 3167–3188, Aug. 2022, doi: 10.1002/ese3.1211.

[35] H. Yan, B. Hu, and R. Wang, “Air-Source Heat Pump for Distributed Steam Generation: A New and Sustainable Solution to Replace Coal-Fired Boilers in China,” *Adv Sustain Syst*, vol. 4, no. 11, Nov. 2020, doi: 10.1002/adsu.202000118.

[36] F. M. Brethomé, N. J. Williams, C. A. Seipp, M. K. Kidder, and R. Custelcean, “Direct air capture of CO2 via aqueous-phase absorption and crystalline-phase release using concentrated solar power,” *Nat Energy*, vol. 3, no. 7, pp. 553–559, Jul. 2018, doi: 10.1038/s41560-018-0150-z.

[37] K. Titus, D. Dempsey, R. Peer, and R. Archer, “Carbon Negative Geothermal: Techno-Economic Analysis of Geothermal Energy combined with Direct and Biomass-Based Carbon Dioxide Removal.”

[38] F. Rosner, A. Schamberger, and H. Breunig, “Techno-economic analysis of a CO 2 direct air capture-cooling tower hybrid process at a geothermal facility.”

[39] G. Leonzio and N. Shah, “Innovative Process Integrating Air Source Heat Pumps and Direct Air Capture Processes,” *Ind Eng Chem Res*, vol. 61, no. 35, pp. 13221–13230, Sep. 2022, doi: 10.1021/acs.iecr.2c01816.

[40] D. M. Snyder, K. F. Beckers, K. R. Young, and B. Johnston, “Analysis of Geothermal Reservoir and Well Operational Conditions using Monthly Production Reports from Nevada and California,” 2017.

[41] O. Bamisile *et al.*, “Geothermal energy prospect for decarbonization, EWF nexus and energy poverty mitigation in East Africa; the role of hydrogen production,” *Energy Strategy Reviews*, vol. 49, p. 101157, Sep. 2023, doi: 10.1016/j.esr.2023.101157.

[42] C. Chen, D. Merino-Garcia, T. D. G. H. Lines, and D. S. Cohan, “Geothermal power generation potential in the United States by 2050,” *Environmental Research: Energy*, vol. 1, no. 2, p. 025003, Jun. 2024, doi: 10.1088/2753-3751/ad3fbb.

[43] M. J. B. Kabeyi and O. A. Olanrewaju, “Central versus wellhead power plants in geothermal grid electricity generation,” *Energy Sustain Soc*, vol. 11, no. 1, p. 7, Dec. 2021, doi: 10.1186/s13705-021-00283-8.

[44] M. J. Barasa Kabeyi and O. A. Olanrewaju, “Geothermal wellhead technology power plants in grid electricity generation: A review,” *Energy Strategy Reviews*, vol. 39, p. 100735, Jan. 2022, doi: 10.1016/j.esr.2021.100735.

[45] A. Kapulluoğlu and M. Gürü, “Electricity production from geothermal sources by binary system; choosing secondary fluids,” *International Journal of Exergy*, vol. 11, no. 1, p. 112, 2012, doi: 10.1504/IJEX.2012.049095.

[46] I. A. THAIN, “1985-1990 Update Report on the Existing and Planned Utilization of Geothermal Energy for Electricity Generation in New Zealand,” *Energy Sources*, vol. 14, no. 2, pp. 205–216, Apr. 1992, doi: 10.1080/00908319208908720.

[47] A. Purkus and V. Barth, “Geothermal power production in future electricity markets—A scenario analysis for Germany,” *Energy Policy*, vol. 39, no. 1, pp. 349–357, Jan. 2011, doi: 10.1016/j.enpol.2010.10.003.

[48] N. Garapati *et al.*, “A Hybrid Geothermal Energy Conversion Technology - A Potential Solution for Production of Electricity from Shallow Geothermal Resources,” *Energy Procedia*, vol. 114, pp. 7107–7117, Jul. 2017, doi: 10.1016/j.egypro.2017.03.1852.

[49] *Negative Emissions Technologies and Reliable Sequestration*. Washington, D.C.: National Academies Press, 2019. doi: 10.17226/25259.

[50] H. Pilorgé, P. Psarras, J. He, and J. L. Wilcox, “Combining Geothermal Potential and Direct Air Capture for Negative Emission Power Generation in California,” 2019.

[51] J. Sekera and A. Lichtenberger, “Assessing Carbon Capture: Public Policy, Science, and Societal Need,” *Biophysical Economics and Sustainability*, vol. 5, no. 3, Sep. 2020, doi: 10.1007/s41247-020-00080-5.

[52] A. Goeppert, M. Czaun, G. K. Surya Prakash, and G. A. Olah, “Air as the renewable carbon source of the future: An overview of CO 2 capture from the atmosphere,” Jul. 2012. doi: 10.1039/c2ee21586a.

[53] H. Azarabadi and K. S. Lackner, “A sorbent-focused techno-economic analysis of direct air capture,” *Appl Energy*, vol. 250, pp. 959–975, Sep. 2019, doi: 10.1016/j.apenergy.2019.04.012.

[54] J. Young *et al.*, “The cost of direct air capture and storage can be reduced via strategic deployment but is unlikely to fall below stated cost targets,” *One Earth*, vol. 6, no. 7, pp. 899–917, Jul. 2023, doi: 10.1016/j.oneear.2023.06.004.

[55] S. Shayegh, V. Bosetti, and M. Tavoni, “Future Prospects of Direct Air Capture Technologies: Insights From an Expert Elicitation Survey,” *Frontiers in Climate*, vol. 3, May 2021, doi: 10.3389/fclim.2021.630893.

[56] A. Kiani, K. Jiang, and P. Feron, “Techno-Economic Assessment for CO2 Capture From Air Using a Conventional Liquid-Based Absorption Process,” *Front Energy Res*, vol. 8, May 2020, doi: 10.3389/fenrg.2020.00092.

[57] A. Sinha, L. A. Darunte, C. W. Jones, M. J. Realff, and Y. Kawajiri, “Systems Design and Economic Analysis of Direct Air Capture of CO2 through Temperature Vacuum Swing Adsorption Using MIL-101(Cr)-PEI-800 and mmen-Mg2(dobpdc) MOF Adsorbents,” *Ind Eng Chem Res*, vol. 56, no. 3, pp. 750–764, Jan. 2017, doi: 10.1021/acs.iecr.6b03887.

[58] B. J. Woodland, A. Krishna, E. A. Groll, J. E. Braun, W. T. Horton, and S. V. Garimella, “Thermodynamic comparison of organic Rankine cycles employing liquid-flooded expansion or a solution circuit,” *Appl Therm Eng*, vol. 61, no. 2, pp. 859–865, Nov. 2013, doi: 10.1016/j.applthermaleng.2013.05.020.

[59] H. X. Wang, B. Lei, and Y. T. Wu, “Control strategies of pumps in organic Rankine cycle under variable condensing conditions,” *Appl Therm Eng*, vol. 234, Nov. 2023, doi: 10.1016/j.applthermaleng.2023.121226.

[60] P. Lu *et al.*, “Design and Optimization of Organic Rankine Cycle Based on Heat Transfer Enhancement and Novel Heat Exchanger: A Review,” Feb. 01, 2023, *MDPI*. doi: 10.3390/en16031380.

[61] R. Perry and D. Green, “Perry’s Chemical Engineers Handbook,” *The McGraw Hill Companies Inc*, 1999.

[62] ASHRAE, *2018 ASHRAE Handbook: Refrigeration*, SI. Atlanta: ASHRAE, 2018.

[63] H. B. Sulistyardi, “An Update on the Basic Design of Lumut Balai Geothermal Power Plant, Indonesia,” 2015.

[64] N. Chagnon-Lessard, F. Mathieu-Potvin, and L. Gosselin, “Optimal design of geothermal power plants: A comparison of single-pressure and dual-pressure organic Rankine cycles,” *Geothermics*, vol. 86, Jul. 2020, doi: 10.1016/j.geothermics.2019.101787.

[65] ASHRAE, “Design Conditions for RENO, NV, USA,” *ASHRAE Handbook*, 2005.

[66] hy-tech Products Inc, “How Much Water Can Flow Through a Pipe (GPM/GPH)?”

[67] Inc. SPX Cooling Technologies, “Cooling Tower Energy and its Management,” Oct. 2016.

[68] S. K. Sanyal, “Classification of Geothermal Systems - A Possible Scheme,” Feb. 2005.

[69] S. J. Zarrouk, B. C. Woodhurst, and C. Morris, “Silica scaling in geothermal heat exchangers and its impact on pressure drop and performance: Wairakei binary plant, New Zealand,” *Geothermics*, vol. 51, pp. 445–459, Jul. 2014, doi: 10.1016/j.geothermics.2014.03.005.

[70] S. K. Sharma, D. Q. Truong, J. Guo, A. K. An, G. Naidu, and B. J. Deka, “Recovery of rubidium from brine sources utilizing diverse separation technologies,” Jun. 15, 2023, *Elsevier B.V.* doi: 10.1016/j.desal.2023.116578.

[71] U.S. Energy Information Administration, “Carbon intensity of U.S. power generation continues to fall but varies widely by state.”

[72] National Renewable Energy Labratory, “Financial Cases and Methods.”

[73] SPX Cooling Technologies, “Cooling Tower Energy and It’s Management,” Oct. 2016.

[74] U.S. Energy Information Administration, “Wholesale Electricity and Natural Gas Market Data.”

[75] U.S. Energy Information Administration, “Annual Energy Outlook 2023.”

[76] United States Environmental Protection Agency, “eGRID Power Profiler,” EPA.gov.

[77] M. Bolinger, J. Seel, C. Warner, and D. Robson, “Utility-Scale Solar, 2022 Edition,” Sep. 2022.

[78] K. An, A. Farooqui, and S. T. McCoy, “The impact of climate on solvent-based direct air capture systems,” *Appl Energy*, vol. 325, Nov. 2022, doi: 10.1016/j.apenergy.2022.119895.

[79] A. Trivella, D. Mohseni-Taheri, and S. Nadarajah, “Meeting Corporate Renewable Power Targets,” *Manage Sci*, vol. 69, no. 1, pp. 491–512, Jan. 2023, doi: 10.1287/mnsc.2022.4354.

APPENDIX

A. VPPA Cost Breakdown

The use of VPPA’s for DAC was considered throughout the analysis however was not included when compared to the independent cases in the results. The DCF used to calculate the LCOE for

DAC for this case is shown in Table A-1 below. The VPPA price used was $46.9/MWh, which is the average strike price over all available VPPAs [79]. Total cost included a demand charge along with a basic charge associated with grid connections needed.

Table A-1: Discounted cash flow for VPPA case.

	-2	-1	0	1	2	3	4
Equipment and Facilities Cost ($)	(0)	(0)	(0)				
Annual Cost ($)	25,718,834	25,718,834	25,718,834	25,718,834	25,718,834	25,718,834	25,718,834
Discount Factor	1.21	1.1	1	0.909090909	0.826446281	0.751314801	0.683013455
Annual Present Value ($)				114,166,640	103,787,855	94,352,595	85,775,086
Operating Costs Net Present Value ($)				23,380,758	21,255,235	19,322,940	17,566,309
	5	**6**	**7**	**8**	**9**	**10**	**11**
Annual Cost ($)	25,718,834	25,718,834	25,718,834	25,718,834	25,718,834	25,718,834	25,718,834
Discount Factor	0.62092132	0.56447393	0.513158118	0.46650738	0.424097618	0.385543289	0.350493899
Annual Present Value ($)	77,977,351	70,888,501	64,444,092	58,585,538	53,259,580	48,417,800	44,016,182
Operating Costs Net Present Value ($)	15,969,372	14,517,611	13,197,828	11,998,026	10,907,296	9,915,724	9,014,294
	12	**13**	**14**	**15**	**16**	**17**	**18**
Annual Cost ($)	25,718,834	25,718,834	25,718,834	25,718,834	25,718,834	25,718,834	25,718,834
Discount Factor	0.318630818	0.28966438	0.263331254	0.239392049	0.217629136	0.197844669	0.17985879
Annual Present Value ($)	40,014,711	36,377,010	33,070,009	30,063,644	27,330,586	24,845,987	22,587,261
Operating Costs Net Present Value ($)	8,194,813.24	7,449,830.21	6,772,572.92	6,156,884.47	5,597,167.70	5,088,334.28	4,625,758.43
	19	**20**	**21**	**22**	**23**	**24**	**25**
Annual Cost ($)	25,718,834	25,718,834	25,718,834	25,718,834	25,718,834	25,718,834	25,718,834
Discount Factor	0.163507991	0.148643628	0.135130571	0.122845974	0.111678158	0.101525598	0.092295998
Annual Present Value ($)	20,533,874	18,667,158	16,970,144	15,427,403	14,024,912	12,749,920	11,590,836
Operating Costs Net Present Value ($)	4,205,234.94	3,822,940.85	3,475,400.78	3,159,455.25	2,872,232.05	2,611,120.04	2,373,745.49
	26	**27**	**28**	**29**			
Annual Cost ($)	25,718,834	25,718,834	25,718,834	25,718,834			
Discount Factor	0.083905453	0.076277684	0.069343349	0.063039409			

Annual Present Value ($)	10,537,124	9,579,204	8,708,367	7,916,697
Operating Costs Net Present Value ($)	2,157,950.45	1,961,773.13	1,783,430.12	1,621,300.11

B. Discounted Cash Flows for Renewable Energy Cases

The discounted cash flows for all the cases shown in the results are outlined below. Various CAPEX and OPEX cost inputs are represented across the 30-year lifetime of the technologies. Economic assumptions for the DCF's are outlined in Table 3-3. These assumptions are held constant for a direct LCOE for DAC comparison across all technologies.

Table B-1: Discounted cash flow for Geothermal+ORC case at 165°C reservoir and 100°C regeneration temperature case.

	-2	**-1**	**0**	**1**	**2**	**3**	**4**
Equipment and Facilities Cost ($)	58,065,242	58,065,242	58,065,242				
Loan Interest Payment ($)	6,967,829	13,935,658	20,903,487	21,114,633	20,825,811	20,513,883	20,177,000
Loan Principle ($)	87,097,863	174,195,726	261,293,589	260,322,638	256,423,536	252,212,505	247,664,592
Annual Cost ($)				12,643,810	12,643,810	12,643,810	12,643,810
Discount Factor	1.21	1.1	1	0.90909090	0.82644628	0.75131480	0.68301345
Annual Present Value ($)				127,073,279	128,416,139	108,562,804	93,355,058
Total Capital Investment + Interest ($)	78,690,016	79,200,990	78,968,729				
Operating Costs Net Present Value ($)				11,494,372	10,449,429	9,499,481	8,635,892
Capital Costs Net Present Value ($)	70,258,942	63,871,766	58,065,242				
	5	**6**	**7**	**8**	**9**	**10**	**11**
Loan Interest Payment ($)	19,813,167	19,420,228	18,995,853	18,537,528	18,042,537	17,507,947	16,930,590
Loan Principle ($)	242,752,846	237,448,160	231,719,099	225,531,714	218,849,337	211,632,371	203,838,047
Annual Cost ($)	12,643,810	12,643,810	12,643,810	12,643,810	12,643,810	12,643,810	12,643,810
Discount Factor	0.62092132	0.56447393	0.51315811	0.46650738	0.42409761	0.38554328	0.35049389
Annual Present Value ($)	81,385,891	73,900,852	67,114,273	57,727,614	49,494,043	44,922,447	40,767,762

Operating Costs Net Present Value ($)	7,850,811	7,137,101	6,488,273	5,898,430	5,362,209	4,874,736	4,431,578
	12	**13**	**14**	**15**	**16**	**17**	**18**
Loan Interest Payment ($)	16,307,044	15,633,614	14,906,310	14,120,822	13,272,495	12,356,301	11,366,812
Loan Principle ($)	195,420,177	186,328,877	176,510,274	165,906,183	154,453,764	142,085,151	128,727,050
Annual Cost ($)	12,643,810	12,643,810	12,643,810	12,643,810	12,643,810	12,643,810	12,643,810
Discount Factor	0.31863081	0.28966438	0.26333125	0.23939204	0.21762913	0.19784466	0.17985879
Annual Present Value ($)	36,992,064	33,560,875	30,442,854	27,609,508	25,034,935	22,695,589	20,570,065
Operating Costs Net Present Value ($)	4,028,707	3,662,461	3,329,510	3,026,827	2,751,661	2,501,510	2,274,100
	19	**20**	**21**	**22**	**23**	**24**	**25**
Loan Interest Payment ($)	10,298,164	9,144,024	7,897,553	6,551,364	5,097,480	3,527,285	1,831,475
Loan Principle ($)	114,300,300	98,719,411	81,892,050	63,718,500	44,091,067	22,893,438	(0)
Annual Cost ($)	12,643,810	12,643,810	12,643,810	12,643,810	12,643,810	12,643,810	12,643,810
Discount Factor	0.16350799	0.14864362	0.13513057	0.12284597	0.11167815	0.10152559	0.09229599
Annual Present Value ($)	18,638,903	16,884,413	15,290,513	13,842,586	12,527,340	11,332,696	10,247,670
Operating Costs Net Present Value ($)	2,067,363	1,879,421	1,708,565	1,553,241	1,412,03	1,283,670	1,166,973
	26	**27**	**28**	**29**			
Loan Interest Payment ($)	0	0	0	0			
Loan Principle ($)	0	0	0	0			
Annual Cost ($)	12,643,810	12,643,810	12,643,810	12,643,810			
Discount Factor	0.08390545	0.07627768	0.06934334	0.06303940			
Annual Present Value ($)	11,336,834	10,306,213	9,369,284	8,517,531			
Operating Costs Net Present Value ($)	1,060,884	964,440	876,764	797,058			

Table B-2: Discounted cash flow for Geothermal+Firm Renewables case at 165°C reservoir and 100°C regeneration temperature.

	-2	-1	0	1	2	3	4
Equipment and Facilities Cost ($)	68,428,650	68,428,650	68,428,650				
Loan Interest Payment ($)	8,211,438	16,422,876	24,634,314	24,883,146	24,542,775	24,175,174	23,778,165
Loan Principle ($)	102,642,976	205,285,951.43	307,928,927	306,784,682	302,189,673	297,227,063	291,867,444
Annual Cost ($)				14,914,176	14,914,177	14,914,177	14,914,177
Discount Factor	1.21	1.1	1	0.909090909	0.826446281	0.751314801	0.683013455

Annual Present Value ($)				156,681,333	157,634,029	133,664,721	115,222,191
Total Capital Investment + Interest ($)	92,734,507	93,336,679	93,062,965				
Operating Costs Net Present Value ($)				13,558,342	12,325,765	11,205,241	10,186,583
Capital Costs Net Present Value ($)	82,798,667	75,271,515	68,428,650				

	5	**6**	**7**	**8**	**9**	**10**	**11**
Loan Interest Payment ($)	23,349,396	22,886,324	22,386,208	21,846,082	21,262,746	20,632,742	19,952,339
Loan Principle ($)	286,079,056	279,827,597	273,076,021	265,784,319	257,909,280	249,404,239	240,218,795
Annual Cost ($)	14,914,176.	14,914,177	14,914,177	14,914,177	14,914,177	14,914,177	14,914,177
Discount Factor	0.62092132	0.56447393	0.513158118	0.46650738	0.424097618	0.385543289	0.350493899
Annual Present Value ($)	100,643,579	91,392,434	83,003,518	71,586,015	61,559,723	55,878,372	50,715,053
Operating Costs Net Present Value ($)	9,260,530.24	8,418,663.86	7,653,330.78	6,957,573.44	6,325,066.76	5,750,060.69	5,227,327.90

	12	**13**	**14**	**15**	**16**	**17**	**18**
Loan Interest Payment ($)	19,217,504	18,423,881	17,566,769	16,641,088	15,641,352	14,561,638	13,395,546
Loan Principle ($)	230,298,514	219,584,612	208,013,597	195,516,901	182,020,469	167,444,323	151,702,085
Annual Cost ($)	14,914,176	14,914,177	14,914,177	14,914,177	14,914,177	14,914,177	14,914,177
Discount Factor	0.318630818	0.28966438	0.263331254	0.239392049	0.217629136	0.197844669	0.17985879
Annual Present Value ($)	46,022,644	41,758,308	37,883,101	34,361,623	31,161,689	28,254,043	25,612,087
Operating Costs Net Present Value ($)	4,752,116.27	4,320,105.70	3,927,368.82	3,570,335.29	3,245,759.36	2,950,690.32	2,682,445.75

	19	**20**	**21**	**22**	**23**	**24**	**25**
Loan Interest Payment ($)	12,136,167	10,776,037	9,307,098	7,720,643	6,007,272	4,156,831	2,158,354
Loan Principle ($)	134,700,468	116,338,722	96,508,036	75,090,895	51,960,383	26,979,429	(0)
Annual Cost ($)	14,914,176	14,914,177	14,914,177	14,914,177	14,914,177	14,914,177	14,914,177
Discount Factor	0.163507991	0.148643628	0.135130571	0.122845974	0.111678158	0.101525598	0.092295998
Annual Present Value ($)	23,211,644	21,030,734	19,049,374	17,249,401	15,614,303	14,129,067	
Operating Costs Net Present Value ($)	2,438,587.04	2,216,897.31	2,015,361.19	1,832,146.54	1,665,587.76	1,514,170.69	1,376,518.81

	26	**27**	**28**	**29**
Loan Interest Payment ($)	(0)	(0)	(0)	(0)
Loan Principle ($)	(0)	(0)	(0)	(0)
Annual Cost ($)	14,914,176	14,914,177	14,914,177	14,914,177
Discount Factor	0.083905453	0.076277684	0.069343349	0.063039409

Annual Present Value ($)	12,780,049	13,999,661	12,726,964	11,569,968
Operating Costs Net Present Value ($)	1,251,380.74	1,137,618.85	1,034,198.96	940,180.87

Table B-3: Discounted cash flow for Geothermal+Grid Electricity case at 165°C reservoir and 100°C regeneration temperature case.

	-2	**-1**	**0**	**1**	**2**	**3**	**4**
Equipment and Facilities Cost ($)	54,641,930	54,641,930	54,641,930				
Loan Interest Payment ($)	6,557,032	13,114,063	19,671,095	19,869,793	19,597,998	19,304,460	18,987,439
Loan Principle ($)	81,962,895	163,925,790	245,888,686	244,974,979	241,305,753	237,342,989	233,063,204
Annual Cost ($)	30,019,010	30,019,011	30,019,011	30,019,011	30,019,011	30,019,011	30,019,011
Discount Factor	1.21	1.1	1	0.90909090	0.82644628	0.75131480	0.68301345
Annual Present Value ($)				107,917,474	110,241,530	92,522,644	75,564,934
Total Capital Investment + Interest ($)	74,050,744	74,531,593	74,313,025				
Operating Costs Net Present Value ($)				27,290,009	24,809,099	22,553,726	20,503,388
Capital Costs Net Present Value ($)	66,116,735	60,106,123	54,641,930				
	5	**6**	**7**	**8**	**9**	**10**	**11**
Loan Interest Payment ($)	18,645,056	18,275,283	17,875,928	17,444,624	16,978,816	16,475,743	15,932,425
Loan Principle ($)	228,441,037	223,449,095	218,057,799	212,235,199	205,946,790	199,155,309	191,820,510
Annual Cost ($)	30,019,010	30,019,011	30,019,011	30,019,011	30,019,011	30,019,011	30,019,011
Discount Factor	0.62092132	0.56447393	0.51315811	0.46650738	0.42409761	0.38554328	0.35049389
Annual Present Value ($)	68,611,991	62,309,661	53,250,049	45,324,225	41,134,699	37,327,296	33,867,255
Operating Costs Net Present Value ($)	18,639,443	16,944,948	15,404,498	14,004,089	12,730,990	11,573,628	10,521,480
	12	**13**	**14**	**15**	**16**	**17**	**18**
Loan Interest Payment ($)	15,345,641	14,711,914	14,027,489	13,288,311	12,489,997	11,627,819	10,696,667
Loan Principle ($)	183,898,927	175,343,617	166,103,882	156,124,968	145,347,741	133,708,336	121,137,779
Annual Cost ($)	30,019,010	30,019,011	30,019,011	30,019,011	30,019,011	30,019,011	30,019,011
Discount Factor	0.31863081	0.28966438	0.26333125	0.23939204	0.21762913	0.19784466	0.17985879
Annual Present Value ($)	30,722,975	27,865,729	25,269,400	22,910,248	20,766,691	18,819,108	17,049,663
Operating Costs Net Present Value ($)	9,564,981	8,695,438	7,904,943	7,186,312	6,533,011	5,939,101	5,399,182
	19	**20**	**21**	**22**	**23**	**24**	**25**
Loan Interest Payment ($)	9,691,022	8,604,926	7,431,942	6,165,120	4,796,951	3,319,330	1,723,498
Loan Principle ($)	107,561,577	92,899,279	77,063,998	59,961,893	41,491,621	21,543,726	0
Annual Cost ($)	30,019,010	30,019,011	30,019,011	30,019,011	30,019,011	30,019,011	30,019,011
Discount Factor	0.16350799	0.14864362	0.13513057	0.12284597	0.11167815	0.10152559	0.09229599

Annual Present Value ($)	15,442,143	13,981,807	12,655,257	11,450,310	10,355,895	9,361,944	8,459,307
Operating Costs Net Present Value ($)	4,908,348	4,462,134	4,056,486	3,687,714	3,352,467	3,047,698	2,770,634

	26	**27**	**28**	**29**
Loan Interest Payment ($)	0	0	0	0
Loan Principle ($)	0	0	0	0
Annual Cost ($)	30,019,010	30,019,011	30,019,011	30,019,011
Discount Factor	0.08390545	0.07627768	0.06934334	0.06303940
Annual Present Value ($)	9,591,913	8,719,921	7,927,200	7,206,546
Operating Costs Net Present Value ($)	2,518,758	2,289,780	2,081,618	1,892,380

LIST OF ABBREVIATIONS

CAPEX	Capital expenditure
CDR	Carbon dioxide removal
CI	Carbon intensity
CO_2	Carbon dioxide
DAC	Direct air capture
DACCS	Direct air carbon capture and storage
DCF	Discounted cash flow
EES	Engineering Equation Solver
EGS	Enhanced geothermal systems

GIS	Geographic information systems
IEA	International Energy Agency
IPCC	Intergovernmental Panel on Climate Change
LCOE	Levelized cost of energy
NGCC	Natural gas combined cycle
OPEX	Operational expenditure
ORC	Organic Rankine cycle
PV	Solar photovoltaic
VPPA	Virtual power purchase agreement
TEA	Techno-economic analysis